Mid- to Late-Holocene Mediterranean climate variability: Contribution of multi-proxy and multi-sequence comparison using wavelet analysis in the northwestern Mediterranean basin

Azuara Julien, Sabatier Pierre, Lebreton Vincent, Jalali Bassem, Sicre Marie Alexandrine, Dezileau Laurent, Bassetti Maria Angela, Frigola Jaime, Coumbourieu-Nebout Nathalie

PII: S0012-8252(20)30278-6

DOI: https://doi.org/10.1016/j.earscirev.2020.103232

Reference: EARTH 103232

To appear in: *Earth-Science Reviews*

Received date: 17 September 2019

Revised date: 5 April 2020

Accepted date: 11 May 2020

Please cite this article as: A. Julien, S. Pierre, L. Vincent, et al., Mid- to Late-Holocene Mediterranean climate variability: Contribution of multi-proxy and multi-sequence comparison using wavelet analysis in the northwestern Mediterranean basin, *Earth-Science Reviews* (2020), https://doi.org/10.1016/j.earscirev.2020.103232

Mid- to Late-Holocene Mediterranean climate variability: Contribution of multi-proxy and multi-sequence comparison using wavelet analysis in the northwestern Mediterranean basin.

Azuara Julien[a,*] Julien.azuara@mnhn.fr, Sabatier Pierre[b], Lebreton Vincent[a], Jalali Bassem[c], Sicre Marie Alexandrine[d], Dezileau Laurent[e], Bassetti Maria Angela[f], Frigola Jaime[g], Coumbourieu-Nebout Nathalie[a]

[a]HNHP, Muséum National d'Histoire Naturelle, UMR CNRS 7194, 75013 Paris, France

[b]EDYTEM, Université Savoie Mont Blanc, UMR CNRS 5204, 7337 Le Bourget du Lac, France

[c]GEOGLOB, Université de Sfax, Faculté des Sciences de Sfax, 3038, Sfax, Tunisia

[d]LOCEAN, Sorbonne Universités (UPMC, Univ Paris 06), UMR CNRS-IRD-MNHN 7159, 75005 Paris, France

[e]Géosciences, Université de Montpellier, CNRS, 34095 Montpellier, France

[f]CEFREM, Université de Perpignan, UMR CNRS 5110, 66000 Perpignan, France

[g]CRG Marine Geosciences, Department of Earth and Ocean Dynamics, Faculty of Earth Sciences, Universitat de Barcelona, 08028 Barcelona, Spain

[*]Corresponding author.

Abstract

Forcings and mechanisms underlying Holocene climate variability still remain poorly. This work review already published paleoclimatic time series and proposes an alternative way to compare them using spectral analysis. Such an approach may emphasize joint features between different signals and lead us closer to the causes of climate changes.

Ten paleoclimatic proxy records from 5 sequences from the Gulf of Lions and surrounding areas were compiled. These paleoclimate time-series were supplemented with proxies of the North Atlantic Oscillations (NAO), El Niño–Southern Oscillations (ENSO) and the Intertropical Convergence Zone (ITCZ) variability. A comparison of their frequency content is proposed using wavelet analysis for unevenly sampled time series. A new algorithm is used in order to propagate the age model errors within wavelet power spectra.

Three main groups of shared features specific to the Mid- and Late Holocene (after 7000 yrs cal BP) can be defined on the basis of the results of these analyses, an Atlantic cyclic period, solar cyclic periods and tropical cyclic periods. The Atlantic cyclic period is probably related to fluctuations of the Atlantic thermohaline circulation which would induce changes in the storm track extension and position thereby impacting upon precipitation and storminess over a millennial scale. The centennial scale solar variability might induce a NAO-like variability of the atmospheric circulation thereby influencing storminess in Western Europe and Mediterranean. Finally, tropical cyclic periods are possibly registered

in of the Gulf of Lions and Atlantic climate proxies, potentially highlighting the influence of ENSO variability over the western Mediterranean.

Keywords: Holocene; Paleoclimatology; Climate dynamics; Mediterranean;Wavelet analysis; Continental biomarkers; Marine biomarkers; Sediment mineralogy; Vegetation dynamics

Introduction

Until recently, the Holocene was often referred to as a stable climatic period. However, with the increasing resolution and diversity of paleoclimatic proxies, Holocene climate variability has progressively come to light. Interest in Holocene climate variability really started in the late 90s, when major features of this period became evident, such as the 8.2 kyrs event (Alley et al. 1997), Bond cycles (Bond et al. 1997, 2001) or the abrupt end of the African Humid Period (deMenocal et al. 2000). The development of this research field has followed increasing interest in current anthropogenic climate change. Indeed, disentangling changes induced by increased greenhouse gases in the atmosphere from the natural centennial scale climate variability is a crucial issue (Stocker et al. 2013).

Holocene rapid climate changes (RCCs) are now reported in many areas all over the world and by numerous types of proxies (Mayewski et al. 2004). Nevertheless, RCCs are not yet fully understood and the comparison of paleoclimatic proxies by simply comparing their curves can be confusing and frustrating when the number of time series increases. However, instead of comparing the paleoclimatic signals in the time/amplitude space it is possible to compare them in the time/frequency plane using non-stationary spectral analysis. In the Atlantic Ocean, one of the most studied areas for this period, an original approach using wavelet analysis describes, in a comprehensive way, the Holocene climate fluctuations through a comparison between different proxies from several sequences using their frequency content (Debret et al. 2007, 2009). Focus on common features in the time/frequency space among different proxies represent an alternative way to draw connections between them and discuss more directly the forcings and the mechanisms underlying reconstructed climate variability. Nevertheless, until recently, wavelet analysis couldn't be applied directly to irregularly sampled times series such as paleoclimate sequences without resampling over interpolated data (Debret et al. 2007, 2009). Such resampling can introduce some biases in the spectral analysis and especially in the statistical analysis of the results (Schulz and Stattegger 1997, Babu and Stoica 2010). Moreover, paleoenvironmental time series are affected by age models' errors which influence on wavelet analysis results are not known.

RCCs are detected by means of numerous proxies all over the Mediterranean basin: vegetation changes (e.g. Jalut et al. 2009, Combourieu-Nebout et al. 2009, Fletcher et al. 2013, Sadori et al. 2015, Jimenez-Moreno et al. 2015, Jaouadi et al. 2016), Sea Surface Temperature (SST) estimates (e.g. Sicre et al. 2016, Jalali et al. 2017), high molecular weight n-alkanes (e.g. Jalali et al. 2017), stable isotope analysis

on speleothems (e.g. Bar-Matthews and Ayalon 2011, Smith et al. 2016), lake level fluctuations (e.g. Magny et al. 2002, 2003, 2007), flood frequencies (e.g. Wirth et al. 2013, Sabatier et al. 2017), thermohaline circulation proxies (e.g. Frigola et al. 2007, Siani et al. 2013), changes in windness (e.g. Costas et al. 2016) or even storminess (e.g. Zazo et al. 2008, Billeaud et al. 2009, Sorrel et al. 2009, Dezileau et al. 2011, 2016, Sabatier et al. 2012, Raji et al 2015, Degeai et al. 2015, Orme et al. 2016), glacier advances (e.g. Giraudi 2005, Giraudi et al. 2011), etc. Nevertheless, while all of these proxies exhibit centennial scale climate variability, the timing of the RCC intervals often differs from one sequence to another. Taken together, these proxies reveal a very complex picture of Holocene climate variability within the Mediterranean Basin. Some authors stress the existence of contrasting geographical patterns, which structure climate variability, and which can partly explain these discrepancies (Roberts et al. 2011, Magny et al. 2012, 2013, Peyron et al. 2013, Jalali et al. 2017). However, even within a restricted area, the correlation between RCC's is not always straightforward and age model uncertainties cannot account for all of the observed differences.

In order to better understand such complex patterns of climate variability in the Mediterranean region, the wavelet analysis approach, initiated by Debret et al. (2007), is further developed and applied to a set of climate proxies from a restricted area, the Gulf of Lions, and over a restricted time period, the Mid- and Late-Holoce. A new wavelet analysis algorithm especially designed for irregularly sampled time series (Lenoir and Crucifix 2018) is used and a new method to propagate age models' errors within wavelet analysis is proposed with a view to improving the reliability of wavelet spectra comparison. The proxies used were produced within the framework of the MISTRALS/PaleoMeX research project. They are supplemented by published sequences from the Balearic Islands, northwestern Spain, the inner Bay of Biscay and time series recording possible drivers (solar variability) or major modes of climate variability (NAO, ENSO). Based on such a dataset, our study aims to identify the external forcings influencing western Mediterranean climate variability over the past 7000 years and to investigate the possible links between the climate variability in this specific key region and the the Atlantic and the tropical areas.

While spectral analysis, including with wavelets, have already been applied to individual Mediterranean paleoclimatic sequences (Fletcher et al. 2013; Siani et al. 2013; Degeai et al. 2015; Dezileau et al. 2016), this study is the first attempt to review and compare the frequency content of several Mediterranean climate proxies. Moreover, a new method for propagating age model uncertainties within wavelet analysis is proposed with a view to improving the reliability of wavelet spectra comparison. We also review elements of climatology that may explain the links we detected between the studied paleoclimatic time series.

Geographical and climatic context

The Gulf of Lions is a crescent-shaped continental margin located in the northwestern Mediterranean basin. It is surrounded by relatively narrow coastal plains and important mountain ranges within the

hinterland of the eastern Pyrenees, the Massif Central and the Southern Alps (Figure 1). The coastal plains are bordered by numerous brackish lagoons that are the result of the interaction between a process of shore line regularization through the migration of sandy barriers, resulting from sediment transfer through littoral hydrodynamics, and the filling of these areas by fluvial and marine inputs (Raynal et al. 2009, Sabatier et al. 2010). The Massif Central and the Southern Alps are separated by the Rhône Valley. The Rhône, one of the major Mediterranean rivers, flows into the Mediterranean Sea in the eastern part of the Gulf of Lions, forming a wide delta and supplying large amounts of sediment (31 Mt yr^{-1}; Ludwig et al. 2009). Its wider drainage basin is influenced by both Mediterranean and temperate climates. The continental margin has a maximum width of 72 km with a water depth ranging between approximately 0 and 100m. Further offshore, the shelf slopes abruptly to the 2000 m deep abyssal plain (Bassetti et al. 2016).

This region is under the influence of a Mediterranean climate with cool mild winters and dry hot summers. In the lowlands, mean annual rainfall ranges from 500 to 800 mm (Rameau et al. 2008) with a maximum in autumn when cumulated October precipitations reach around 80mm, and a minimum in summer with cumulated July precipitations of less than 20mm (Météo France data). Mean annual temperature is between 12-16°C (Rameau et al. 2008) with a maximum of around 23°C in July (monthly average) and a minimum of around 7°C in January (monthly average) (Météo France data). However, the steep altitudinal gradient results in a decrease of seasonality with altitude. July precipitation and mean temperature increase and decrease respectively in the mountains.

Large scale circulation patterns over the North Atlantic and Europe directly influence the western Mediterranean (Plaut and Simmonet 2001). Persistent high-pressure systems over the Arctic regions (Greenland, Iceland) and over Scandinavia tend to advect more Atlantic lows and rainfall toward the western Mediterranean. In contrast, when the Atlantic subtropical anticyclone (Azores high) shifts northwards, precipitation decreases. These large-scale circulation patterns also influence wind circulation. An anticyclonic blocking over the eastern Atlantic, associated with a low-pressure system over the central Mediterranean, induces cold, dry, northerly winds over the Gulf of Lions (Mistral and Tramontane, Figure 1) (Najac et al. 2009; Sicre et al. 2016), while persistent high-pressure systems over Scandinavia induce warm, humid, south-easterly winds (Plaut and Simonet 2001). Finally, large scale circulation patterns can contribute to the triggering of extreme climate events such as Heavy Precipitation Events (HPE; <200mm in a day) (Joly et al. 2012, Nuissier et al. 2011) or summer heat waves (Cassou et al. 2005). Latitudinal shifts of the Atlantic zonal storm track associated with this general atmospheric circulation also influence the frequency and the intensity of northern Mediterranean cyclones (Trigoal and DaCamara 2000) (Figure 1).

The complex orography of the northwestern Mediterranean basin and the interactions between the hinterland and the Mediterranean Sea promote mesoscale convective systems and greatly contribute to the regional climate specifics of this area. The Mediterranean Sea represents an important source of heat

and moisture (Winschall et al. 2014). Warm and humid air advection from the Mediterranean towards the upland areas surrounding the Gulf of Lions causes significant rainfall and sometimes leads to HPE, such as that which occurred in the Gard on the 8-9 September 2002, when 600mm of rain fell in 24 hours (Nuissier et al 2011). The Gulf of Genoa is one of the major cyclogenesis regions of the whole Mediterranean basin and one of the most persistent throughout the year (Figure 1). The Gulf of Lions and the Balearic Islands, which are situated a few hundred kilometers to the west, are secondary centers of cyclogenesis linked to this very active and persistent center (Trigo et al. 1999, Lionello et al. 2016). Moreover, mesoscale cyclones formed in the Gulf of Genoa promote Mistral and Tramontane winds over the Gulf of Lions (Lebeaupin Brossier and Drobinski 2009).

Inter-annual climate variability in the western Mediterranean is greatly influenced by major patterns of atmospheric variability defined by differences in seasonal average sea-level pressures (SLP) at chosen locations. One of the most important is the North Atlantic Oscillation pattern (NAO) which involves inter-annual differences in the seasonal mean SLP between the Azores high and the Icelandic low (Hurrell et al. 2003). This pattern of variability is thus related to the strength of the meridional pressure gradient along the North Atlantic sector. Years characterized by a positive (negative) NAO index display a higher (or lower) meridional pressure gradient which caused stronger (or weaker) westerlies. NAO variability has a considerable influence on the activity of the North Atlantic storm track during winter time (Rogers 1997, Hurrell et al. 2003). As a consequence, winter precipitation in the western-Mediterranean basin is higher and cyclogenesis is more pronounced during negative NAO years. The Mediterranean Oscillation pattern, involving contrasting pressure conditions between the western and the eastern Mediterranean, is a regional manifestation of the NAO (Conte et al. 1989). In addition, the Western Mediterranean Oscillation index (WeMOi), defined as the difference in pressure values between the Azores high and the Ligurian low systems, has been shown to detect variability in cyclogenesis in the western Mediterranean basin and thus is more effective that NAO for explaining seasonal precipitation in this area, especially on the east margin of the Iberian Peninsula (Martin-Vide and Lopez-Bustins 2006). The Scandinavian pattern (SCAND) is another important mode of inter-annual variability in the northern hemisphere, influencing the climate of the western Mediterranean region. It is defined as the SLP differences between Scandinavia and both Western Europe and Mongolia. Strong persistent positive pressure anomalies over Scandinavia cause enhanced precipitation in the central and western Mediterranean (Bueh and Nakamura 2007). Finally, the El Niño Southern Oscillation (ENSO), which affects the tropical Pacific and Indian oceans, also impacts upon the European climate including that of the western Mediterranean area (Brönnimann et al. 2007). In winter, El Niño events can induce an atmospheric circulation pattern resembling a negative NAO, increasing winter precipitation rates in the western Mediterranean, but with sea level pressure anomalies shifted north-eastward. On the other hand, la Niña events can lead to a quasi-symmetric response, decreasing winter precipitation in the western Mediterranean (Brönnimann et al. 2007). In contrast, in Spring, El Niño events may induce a contrasting pattern characterized by dryer conditions in the western

Mediterranean and wetter conditions in the area stretching from north-western Europe to the north western Iberian Peninsula; the opposite occurs during la Niña events. Nevertheless, it must be noted that these typical responses of European climate to ENSO are not always well recorded (Brönnimann et al. 2007). The ENSO signal in Europe is rather non-stationary and further work is needed to better characterize its modulating factors especially on decadal and multidecadal time-scales (Brönnimann et al. 2007).

Furthermore, the Gulf of Lions is one of the few areas where deep water formation occurs in the Mediterranean basin (MEDOC group 1970). Mediterranean waters are stratified in three different layers, i.e. surface, intermediate and deep waters. The surface waters (0-200m) originate in the Atlantic and flow eastwards through the Strait of Gibraltar becoming progressively warmer and saltier (Modified Atlantic Waters, MAW) (Figure 1). The intermediate waters (200-500m) form in the eastern Mediterranean during the winter season when dry, cold air from Anatolia causes surface waters to sink (Levantine Intermediate Waters, LIW) (Figure 1). Finally, the deep waters (>500m) form in the northern part of the Mediterranean basin where MAW is cooled by winds and mixed with until they reach bottom water density and sink towards the abyssal plains (Western Mediterranean Deep Water, WMDW) (Rhein 1995, Schroeder et al. 2010). In the Gulf of Lions, the dry and cold Mistral and Tramontane winds are responsible for deep water formation (Figure 1). The Mistral blows from the north following the Rhône valley while the Tramontane blows from the north west through the plain between the Pyrenees and the Massif Central. They both cause surface water heat loss within the gulf and thus lead to relatively low SST compared to the rest of the Mediterranean basin (Sicre et al. 2016). In summary, the climate of the Gulf of Lions results from the complex interactions between remotely driven processes and local features.

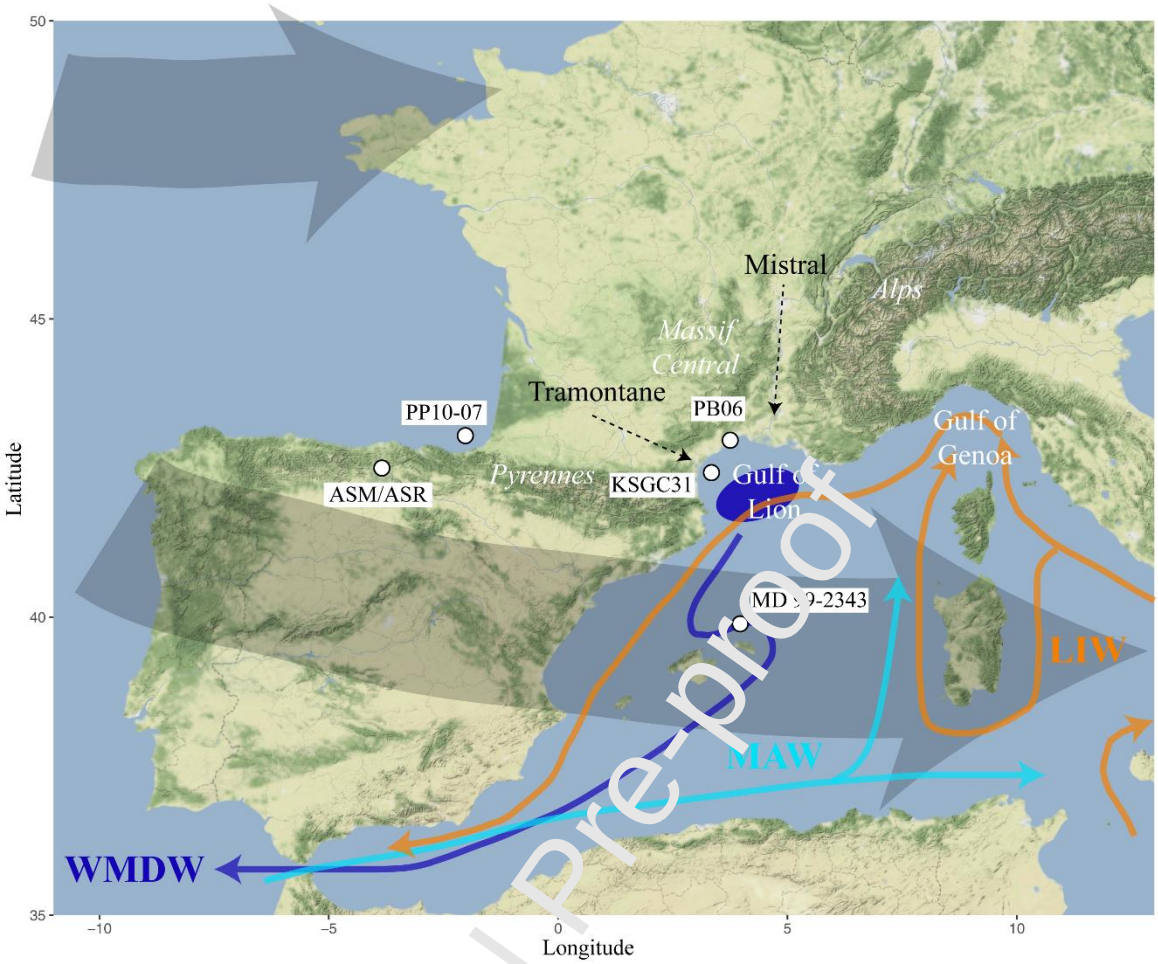

Figure 1: Locations of studied core sequences. Thin colored arrows represent marine currents (MAW, Modified Atlantic Waters; WMDW, Western Mediterranean Deep Waters; LIW, Levantine Intermediate Waters), black dotted arrows represent winds of southern France, and large shaded grey arrows represent the southern part of the Atlantic storm track. The blue oval represents the zone of formation of Western Mediterranean Deep Waters (WMDW).

Method

The non-stationarity of Holocene climate variability has been highlighted by numerous studies based on diverse proxies and is crucial to understand the physical mechanisms at play and the role of external forcings (Debret et al. 2007, 2009). Wavelets are tools for spectral analysis of non-stationary time series that allows us to determine the dominant modes of variability embedded in a signal and how these modes vary over time (Torrence and Compo 1998). In this article, we assume that two signals who shares statistically significant features in the time/frequency space may be linked in some way and we review the mechanism which could explain such a link. It is important to note that, wavelet analysis allows to characterize pseudo-periodic and non-periodic oscillations just as well as fully periodic oscillations. Here, we are only looking for significant shared features in the wavelet spectra of the studied

paleoclimatic time series which can highlight a connection between them whether these features are periodic or pseudo-periodic.

Evenly spaced time series are usually needed to perform wavelet analysis (Torrence and Compo 1998) and paleoclimatic sequences have thus to be re-sampled with a constant time-step before performing classical wavelet analysis (Debret et al. 2007). However, such re-sampling can introduce unpredictable biases in the results of spectral analysis (Lenoir and Crucifix, 2018a and b). Fortunately, alternative exist to perform wavelet analysis on irregularly samples time series without any re-sampling (Foster 1996, Mathias et al. 2004, Lenoir and Crucifix 2018b). However, for now, the WAVEPAL python package we used to perform wavelet analysis on irregularly sampled time series doesn't allow to perform cross-wavelet analysis to highlight shared spectral features between different signal. Thus, in this article we compare directly the scalograms of the different time series.

Wavelet analysis, generalities

Wavelets are wave functions with zero mean and localized in both time and frequency domain (Admissibility conditions, Farge 1992): this means that they rapidly approach zero after few oscillations and they contain only one period known as the wavelet scale. In this article, wavelets derived from the Morlet mother wavelet are used:

$$\psi_0(\eta) = \pi^{-1/4} e^{i\omega_0 \eta} e^{-\eta^2/2}$$

The input η is a non-dimensional time parameter and ω_0 is the non-dimensional frequency, here equal to 5,5 to have the finest time resolution while satisfying the admissibility conditions (see Lenoir and Crucifix 2018b). The Morlet wavelets are widely used for paleoclimatic time series analysis and more generally for geophysical and ecological data.

The continuous wavelet transform of a discrete time series x_n is defined as the convolution of x_n with a wavelet function. Because wavelet scales are linked to Fourier periods, by varying the scale and the time index, wavelet transforms allow to examine the contribution of a set of periods to the signal variability all along the time series. The results are presented in the form of a scalogram, a graph with time in abscissa, periods or scales in ordinate and the wavelet power (square modulus of the wavelet transform) color coded. A perioc or pseudo-periodic signal of period λ which contribute to signal variability within the time interval $[t_1, t_2]$ is characterized by a power local maximum centered on λ between t_1 and t_2, we called it a cyclic period.

Wavelet analysis of irregularly sampled time series

In this study, the wavelet analysis are performed with the WAVEPAL python package which allow to carry time-frequency analysis of irregularly sampled time series (Lenoir and crucifix 2018 a and b). As recommended when studying the periodic component of a signal rather than its background noise, a weighted smoothed scalogram is computed from each of the selected paleoclimate time series (Lenoir

and Crucifix 2018b). The smoothing coefficient $\gamma = 0.5$ has been choosen for all the sequences, the length of smoothing per scale is fixed and the coefficient for the scale resolution is $\delta j = 0.05$.

The scalogram defined by Lenoir and Crucifix (2018b) differs slightly from the scalogram defined classically for evenly spaced time series (Torrence and Compo 1998). Nevertheless, when applied to regularly sampled data it gives very similar result to what is obtain with the "classical" approach (Lenoir and Crucifix 2018b).

Significance testing

The significance of the cyclic periods discussed in the article is evaluated with the analytical approach proposed by Lenoir and Crucifix (2008b) and using the WAVEPAL and CARMA pack python packages (Lenoir and Crucifix 2018 a and b). The background stationary noise of time series are modeled using a CARMA (1,0) process, that is to say a red noise and the confidence levels are computed after detrending the data using polynomial trends. According to the recommendation made by Lenoir and Crucifix (2018b) we fix at 2 the number of conserved moments in the gamma-polynomial distribution used to approximate a linear combination of independent chi-square distributions.

Edge effects

Near the edge of the time series, in an area which length increase with the scale, part of the wavelet supports can stand outside bounds of the data (Lenoir and Crucifix 2018b). This area is called the "cone of influence" and is shaded with grey on both sides of the scalograms. Within the cone of influence, wavelet power amplitude is likely to be underestimated (Torrence and Compo 1998).

In the case of irregularly sampled time-series, the scale of the wavelet packet may be too low compared to the local time step, leading to the erroneous detection of high frequency periodicities which are not present in the signal. This bias called aliasing can be prevented by excluding from the wavelet analysis some areas of the time-scale plane (Lenoir and Crucifix 2018b). These excluded areas form the Shannon-Nyquist exclusion zone (SNEZ), with reference to the Shannon-Nyquist sampling theorem from which they are calculated. The SNEZ is represented in black at the bottom of the scalograms. Due to the correlation between neighboring scales and to the smoothing in the scalogram, the SNEZ must be slightly extended (Lenoir and Crucifix 2018b). In the scalograms, this extension of the SNEZ is the shaded grey area just above the SNEZ.

Finally, according to the recommendation in Lenoir and Crucifix (2018b), we choose a fixed length of integration when computing the weighted smoothed scalogram. This results in two more excluded area in black at the right and the left of the scalogram.

Propagation of age model uncertainties in wavelet analysis

Most paleoclimatic sequence chronologies are based on radionuclide measurements and are therefore affected by age model uncertainties. These uncertainties introduce an inherent bias within all types of spectral analysis. In most of the papers dealing with spectral analysis of paleoclimatic sequences this problem is not considered and not even mentioned. Even if there is no way to avoid this bias, it is

possible to quantify it. For this study, a short program based on a Monte Carlo method has been written to propagate age model errors within wavelet analysis.

For each sequence, 3000 alternative age models without age reversals are generated from the corresponding radiocarbon dates, their errors at one sigma, the calibration curve and the local reservoir age. All of the alternative age models are computed using functions derived from clam code in R (Blaauw 2010) and always with the same parameters. Wavelet power spectra are calculated for each alternative age model. The wavelet power spectrum of the original time series is used to define time slices and peaks of interest corresponding to significant periods. An algorithm of local maxima detection is run to find the position of the peaks of interest within the 3000 alternative wavelet spectra and the 5th and the 95th quantiles of the result are used to define the 95% confidence interval of each peak. Such a Monte Carlo method for propagating age model uncertainties has already been used by Anchukaitis and Tierney (2013) to compute empirical orthogonal function analysis on proxies from different sequences. This age-model error propagation allows a more reliable comparison between wavelet power spectra from different paleoclimatic time-series. Nevertheless, because the speleothem record from the Asiul Cave (see below) is a composite time series, it was not possible to use the age model error propagation algorithm with the available data.

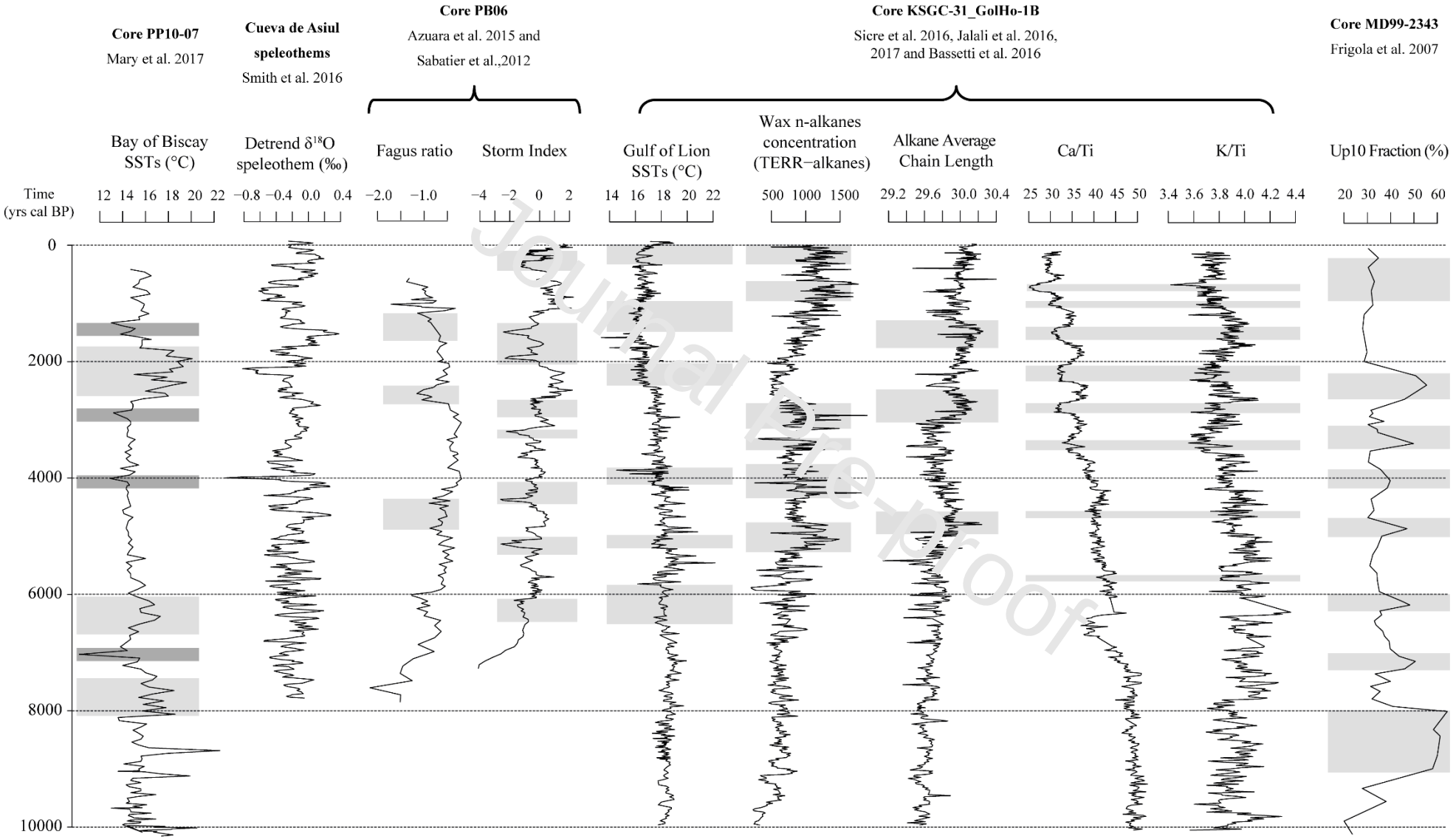

Figure 2: Curves of the studied time series. Shaded grey boxes represent RCCs defined by the authors

Figure 2: Curves of the studied time series. Shaded grey boxes represent RCCs defined by the authors3

Data sets and results

This section summarizes the context, the chronological framework and the meaning of the climate proxies used in this study; it also describes briefly their main features in the frequency domain. The original curves of the studied sequences are presented in Figure 2. Because a full description of the wavelet power spectra would be tedious and redundant given the scalograms represented in the Figure 3, only the significant periodicities are considered.

PB06 core and the Palavasian lagoon system

The Palavasian lagoon system is located in southern France (Figure 1) along the coast of the Gulf of Lions. The wetland complex consists of seven shallow ponds (depth <1m) (Dezileau et al. 2005). These hypersaline, back-barrier lagoons are separated from the Mediterranean Sea by a wave-produced, sandy barrier measuring 150 m wide and rising to a height of 2–3m above the mean sea level. Tidal variability is modest (with a mean range of 0.30 m), which minimizes the influence of dynamic tidal currents. The study site is located along the southeastern-facing shoreline and is extremely vulnerable to intense storms blowing in from the south and southeast (Dezileau et al. 2005, 2011).

A 7.9 m long core (PB06) was recovered from Pierre Blanche Pond in 2006 (Dezileau et al. 2011, Sabatier et al. 2010, 2012). The chronology was established using 19 Accelerator Mass spectrometry (AMS) radiocarbon dates on monospecific shell samples of Cerastoderma glaucum. Dates were calibrated using the Intcal09 calibration curve and the radiocarbon reservoir ages were estimated in relation to historical events and paleoenvironmental changes (Sabatier et al. 2010b). For the last centuries, historical storm events, together with short-lived radionuclide measurements, were also used (Sabatier et al. 2012).

Sedimentological analysis

Several analyses were performed on core PB06. Clay minerals were identified and quantified by X-ray diffraction (XRD) and X-ray fluorescence analyses were also performed to estimate Al, Si, S, Cl, K, Ca, Ti, Mn, Fe, Zn, Br, Sr, Rb, and Zr contents (Sabatier et al. 2012). The macrofauna content was estimated by sieving samples at 1mm and identifying the shells every 2cm in order to identify lagoonal and marine species (Sabatier et al. 2012).

Storms are frequent in the northern Mediterranean during the wet season (October to March) and the most powerful ones are able to break the sandy barriers of coastal lagoons causing marine sediments to enter the ponds and creating what are called overwash fans as illustrated in Sabatier et al. (2008). Thus, sedimentological archives from coastal lagoons potentially represent long term records of past intense storms. Distal overwash fans are clearly identified in PB06 through the presence of marine mollusk

shells (M), changes in clay mineralogy (C) and increases in the Zr/Al ratio (Z). On the basis of this sedimentological evidence, several periods of intense storm activity have been defined (Figure 2) (Sabatier et al. 2012). For the purpose of this study, all of these indicators of past storm activity were combined to sum up all of the information within one unique time series called the "Storm Index" (SI):

$$SI(t) = -C(t) + 3 \times \frac{M(t)}{max(M)} + 3 \times \frac{Z(t)}{max(Z)}$$

The M and Z time series are scaled by dividing them by their maxima, $max(M)$ and $max(Z)$, and then multiplying them by a factor 3 to have an amplitude of variation of about the same order of magnitude as the C time series. High SI values correspond to periods of frequent storms while low SI values correspond to periods with fewer storms.

The SI record from the Palavasian lagoon covers the last 7300 yrs with a mean temporal resolution of about 20 yrs. After 4000 yrs cal BP, a major significant cyclic period of 1536-1590 yrs arises and continues until the end of the Holocene. Between 2500 and 1500 yrs cal BP, a significant cyclic period of 692-768 yrs is recorded. A cyclic period of 370-426 yrs is evidenced around 2000 yrs cal BP. Finally, a significant cyclic period of 167-220 yrs is recorded at around 5500 and 500 yrs cal BP (Figure 3).

Paleoecological analysis

For pollen extraction, samples were sieved, processed with HCl and HF for mineral digestion and sodium polytungstate for density separation. Pollen concentration was estimated by adding a known amount of Lycopodium spores. Pollen grains were counted and identified at 400x and 1000x amplification, respectively, with reference to pollen keys, atlases and comparison with a reference collection (Azuara et al. 2015, 2018).

In the French Mediterranean Mountains, *Fagus sylvatica* and *Abies alba* are at the limit of their geographical range. Thus, both taxa are particularly sensitive to climate fluctuations. Decreases (increases) in pollen proportions of these two taxa synchronous with increases (decreases) in deciduous *Quercus* proportions have been interpreted as repetitive mountainous forest retreats toward higher altitudes coinciding with repeated expansions of deciduous *Quercus* at lower altitudes during dry events (Azuara et al. 2015, 2018). The covariations of these taxa are summarized within a single indicator called "Aridity index" (A_i):

$$A_i = log\left(\frac{F_p + A_p}{Q_p}\right)$$

F_p, $A_p$and Q_p are respectively *Fagus*, *Abies* and deciduous *Quercus* pollen proportions. An increase in A_i indicates increasing aridity recorded by the vegetation.

The aridity index time series ranges from 570 to 7800 yrs cal BP with a mean temporal resolution of about 60 yrs. Before 5000 yrs cal BP, a significant cyclic period of 1305-1351 yrs prevails in the signal, while after 4000 yrs cal BP, a significant cyclic period of 1911-1978 yrs is rather recorded. Two significant cyclic periods of 430-832 yrs and 1097-1218 are recorded between 2000 and 3000 yrs cal

BP (Figure 3). The two significant cyclic periods of less than 400 yrs at the ends of the sequence will not be discussed as they are relatively short cycles compared to the mean time step and they have a poor chronological extension.

KSGC-31_GolHo-1B composite core and the inner shelf of the Gulf of Lions

The KSGC-31_GolHO-1B sequence is composed of two cores retrieved from the same site on the inner shelf of the Gulf of Lions (Bassetti et al. 2016, Jalali et al. 2016, 2017) (Figure 1). In this part of the inner shelf, sediments predominantly come from the Rhône river mouth where they are advected along the coast by longshore drift thereby forming the Rhône mud belt (Bassetti et al. 2016). The chronology of the KSGC-31_GolHO-1B sequence is based on 21 AMS radiocarbon dates on mollusk shells and 210 Pb measurements. Dates were calibrated using CALIB7.1 software and the MARINE13 calibration curve with a local marine reservoir age of $\Delta R = 23 \pm 71$ years (Jalali et al. 2016, Bassetti et al. 2016).

XRF analysis

Core KSGC-31 was split into two parts and scanned with an XRF core scanner (IFREMER) to produce semi-quantitative estimates of major and minor element abundances within the sediments with a high resolution, one-centimeter step measurement. The results were expressed as element to element ratios and the resulting time series ranges from 110 to 10 050 yrs cal BP with a mean temporal resolution of about 15 yrs (Bassetti et al. 2016).

The Ca/Ti ratio is considered to record biogenic marine productivity, marked by the Calcium abundance, versus terrigenous inputs, marked by the Titanium content. This proxy displays two main significant cyclic periods of 1771-1965 yrs before 4000 yrs cal BP and 626-694 yrs after 4000 yrs cal BP (Figure 3).

On the other hand, the abundance of potassium in the sediments is related to the abundance of illite. Since the potassium abundance within illite minerals decreases as a function of pedogenetic processes, the K/Ti ratio is used as an indirect proxy of chemical weathering and thus of soil formation. High ratio values highlight erosion of surface soil horizons, while low values reflect erosion of deep soil horizons. This time series shows one main cyclic period of 1210-1342 yrs which, though clearly visible throughout the Holocene, is more significant at the base and at the top of the sequence. A second cyclic period of 430-832 yrs is visible between 6500 and 3000 yrs cal BP (Figure 3).

Biomarker analysis

Biomarker analyses were performed continuously at a sampling step interval of 1 centimeter all along the sequence. Lipids were extracted from the frozen and dried sediments with dichloromethane and methanol. Alkenones and n-alkanes were isolated using silica gel chromatography and quantified using gas chromatography. The time series derived from these biomarker analyses covers the last 10 000 yrs with a mean temporal resolution of about 15 yrs (Jalali et al. 2016).

Unsaturation ratio of C37 alkenones was converted into Sea Surface Temperature (SST) using the calibration developed by Conte et al. (2006) (Sicre et al. 2016). The scalogram displays a significant

cyclic period of 2241-2320 yrs from 8000 yrs cal BP to the present. Two significant cyclic periods of respectively 541-643 and 541-621 yrs are evident between 5500 and 6000 yrs cal BP and around 2250 yrs cal BP repsectively. Finally, a significant cyclic period of 140-252 yrs is recorded around 4500 yrs cal BP (Figure 3).

High-molecular-weight n-alkanes with an odd carbon number, i.e. C27+C29+C31+C33 homologs (TERR-alkanes), were quantified in order to track terrigenous inputs from the Rhône River (Jalali et al. 2016). Indeed, these compounds are constituents of epicuticular leaf waxes and their accumulation in the sediments of the Gulf of Lions is primarily associated with vegetation cover changes and soil erosion in the Rhône river catchment. The wavelet analysis presents two cyclic periods of 1862-1928 yrs and 998-1069 yrs between 6000 yrs cal BP and the present. Then, short cyclic periods of about 250-300 yrs are registered around 9000, 6000, 3000 and 600 yrs cal BP (Figure 3).

Finally, the n-alkane Average Chain Length (ACL) was calculated between C_{27} and C_{33} in order to derive information on changing moisture conditions and associated vegetation types in the Rhône watershed (Jalali et al. 2017). Under conditions of water deficit, plants actually produce longer chain n-alkane to minimize water loss through evapo-transpiration (Gagosian and Peltzer, 1986). The scalogram of the ACL time series displays a major significant cyclic period of 2293-2374 yrs between 8000 and 4000 yrs cal BP. Two cyclic periods of 1107-1187 and 730-1065 yrs are also recorded after 3000 yrs cal BP. Two short cyclic periods of 419-516 and 267-681 yrs are evidenced around 5500 and 1000 yrs cal BP (Figure 3).

MD 99-2343 core and the Balearic Islands

The MD 99-2343 core was recovered north of Minorca Island, at 2391 m water depth within the Minorca sediment drift (Figure 1) (Frigola et al. 2007). Western Mediterranean Deep Waters (WMDW) formed in the Gulf of Lions, flow southward and are deviated eastward by the Balearic promontory (Figure 1). The steep slope results in a change of direction and an intensification of the current. This leads to the formation of a depression filled by coarse sediments while the fine fraction escapes out of the depression and contributes to the formation of an associated sediment drift parallel to the promontory (Frigola et al. 2007). The chronology of this part of the core is based on 10 AMS radiocarbon dates performed on multi- and monospecific planktonic foraminifera shells plus a tie point (the onset of the Holocene) defined by correlation with the oxygen isotope record of the Greenland ice core GISP2 (Frigola et al. 2007). Ages were calibrated using the MARINE04 calibration curve with a radiocarbon reservoir age of 408 yrs and a regional marine reservoir of $\Delta R = 76$ years average over the western Mediterranean basin (Stuiver and Reimer, 1993).

Sedimentological analysis

One-centimeter thick sediment samples were taken every 4 to 6 centimeters. Grainsize was measured using a laser diffraction size analyzer on the non-carbonate fraction after removal of organic matter and carbonate. The volume percentage of the fraction coarser than 10µm (Up 10 fraction) was quantified as

an indicator of deep current variability at the site. Therefore, the Up 10 fraction sequence from the MD 99-2343 core provides a proxy of the WMDW current strength over the last 12000 yrs with a mean temporal resolution of about 150 yrs (Frigola et al. 2007).

Due to this long mean time step, the picture of the frequency content given by the wavelet analysis is coarse. The early Holocene is characterized by a cyclic period of about 568-725 yrs which shifts toward longer cycles of 990-1099 yrs between 8000 and 5000 yrs cal BP. During the second part of the Holocene, two short cyclic periods of 750-924 yrs and 1450-1554 yrs cycles dominate the signal variability. The major cyclic period of about 3000 at the beginning of the time series is caused by significant non-periodic fluctuation of the Mediterranean overturning circulation at the onset of the Holocene (Figure 3).

The speleothems of "Cueva de Asiul"

Smith et al. (2016) recovered two sequences from speleothems labeled ASR and ASM in the Cueva de Asiul, a closed karstic depression in the Cantabrian Cordillera in northwestern Spain (Figure 1). The chronologies of these sequences rely on 10 and 12 U/Th dates respectively. Speleothem ASR grew between 12500 and 500 years BP with a long interruption between 8600 and 4000 years BP. Speleothem ASM grew between 7850 and 0 yrs BP with an interruption between 3800 and 2150 years BP and thus almost entirely spans the gap in the ASR record (Smith et al. 2016 Supplementary information).

Geochemical analysis

Smith et al. (2016) performed calcite $\delta^{18}O$ analysis using an IsoPrime isotope ratio mass spectrometer to track precipitation changes throughout the Holocene. The reliability of the two records within their overlapping period was tested by cross correlation analysis and they were then combined within a single detrended time series (Smith et al. 2016 Supplementary information). The data for this combined and detrended time series were downloaded from the NOAA database for use in our study (https://www.ncdc.noaa.gov/paleo-search/study/20082).

A monitoring study in Cueva de Asiul demonstrates that the cave's hydrological system is recharged primarily by winter rainfall and that the isotopic composition of the cave drip waters reflects the $\delta^{18}O$ composition of winter rainfall from the preceding year (Smith et al. 2016 b). Therefore, $\delta^{18}O$ measurements on ASR and ASM speleothems may represent winter rather than annual past precipitation rates over the last 7800 yrs with a mean temporal resolution of 15 yrs. The scalogram of this time series displays a frequency content dominated by a cyclic period of about 1400 years between 5000 yrs cal BP and the present. Short cyclic periods of about 200-450 yrs are also recorded around 500, 1500, 2000 and 4500 yrs cal BP respectively (Figure 3).

The Bay of Biscay SST

Mary et al. (2017) studied the PP10-07 core recovered in the inner Bay of Biscay, at a point between the Aquitaine shelf and the Cantabrian shelf. The Bay of Biscay is characterized by a complex oceanic circulation. This area is particularly sensitive to North Atlantic subpolar and subtropical gyre dynamics.

The chronology of the sequence is based on 10 AMS radiocarbon dates on planktonic foraminifera (Mary et al. 2017). Dates were calibrated using the MARINE13 calibration curve with a radiocarbon reservoir age of 405yrs (Reimer et al. 2013). The age model was obtained by a smooth-spline regression (Mary et al. 2017).

SST reconstructions

Mary et al. (2017) derived SSTs from the planktonic foraminifera abundances within the >150µm sediment fraction using the Modern Analogues Technique (Mary et al. 2017). The Annual SST data from the PP10-07 core were retrieved from the Pangea database to be used within our study (https://doi.pangaea.de/10.1594/PANGAEA.872166). This time series covers the last 10 000 yrs with a mean temporal resolution of 50 yrs. Colder and warmer SST periods are recorded in the Bay of Biscay. They are related to variations in heat transport from the tropics toward Western Europe, due to changes in past dynamics of the Atlantic gyres (Mary et al. 2017).

The wavelet analysis of Bay of Biscay SSTs shows a cyclic period of 1305-1398 yrs throughout the first half of the Holocene. After 6000 yrs cal BP, a cyclic period of 1606-1782 yrs dominates the signal variability. Two short cyclic periods of 388-494 and 123-203 yrs are evidenced around 9000 and 2000 yrs cal BP (Figure 3).

Complementary time series

In order to identify the periodicities highlighted in the proxies presented above, some supplementary time series were also analyzed. These series are not necessarily coming from areas neighboring the Gulf of Lions, but they display a number of common features with the studied sequences.

Solar activity proxy

Two time series for reconstructed solar activity throughout the Holocene are available: Sunspot Number (SN) estimates from a dendro-chronologically dated ^{14}C record (Solanki et al. 2004) and Total Solar Irradiance (TSI) estimates from several cosmogenic isotope records (Steinhilber et al. 2012). Since these two time series display very similar frequency contents and since the SN time series have a better time resolution, it was decided to use the latter to investigate the presence of solar periodicities in the studied paleoclimate sequences (ftp://ftp.ncdc.noaa.gov/pub/data/paleo/climate_forcing/solar_variability/solanki2004-ssn.txt).

NAO index records

Three NAO Index records were used to investigate the link between certain observed variability patterns and the NAO variability:

- The NAO index reconstruction by Olsen et al. (2012) using a lake record from Greenland and ranging from 300 to 5200 yrs cal BP (ftp://ftp.ncdc.noaa.gov/pub/data/paleo/paleolimnology/greenland/lake-ss1220-2012.txt).
- The NAO index reconstruction by Trouet et al. (2009) using a tree-ring drought reconstruction from Morocco and a speleothem-based precipitation proxy from Scotland and covering the last

millennium (NOAA database: ftp://ftp.ncdc.noaa.gov/pub/data/paleo/treering/reconstructions /nao-trouet2009.txt).

- The model-constrained NAO index reconstruction by Ortega et al. (2015) using 9 paleoclimate proxies distributed around the Atlantic Ocean and also covering the last millennium (NOAA database: https://www1.ncdc.noaa.gov/pub/data/paleo/contributions_by_author/ortega2015/ortega2015nao.txt).

Tropical climate variability

Two paleoclimate time series from tropical regions, and displaying common periodicities with the Gulf of Lions sequences, were used to address the question of the influence of ENSO variability on the northwestern Mediterranean area: the ENSO variability record from the Ecuadorian Andes published by Moy et al. (2002) (NOAA database : ftp://ftp.ncdc.noaa.gov/pub/data/paleo/paleolimnology/ecuador/pallcacocha_red_intensity.txt) and the ICTZ position record from the Cariaco Basin published by Haug et al. (2001) (PANGEA database : https://doi.pangaea.de/10.1594/PANGAEA.81965).

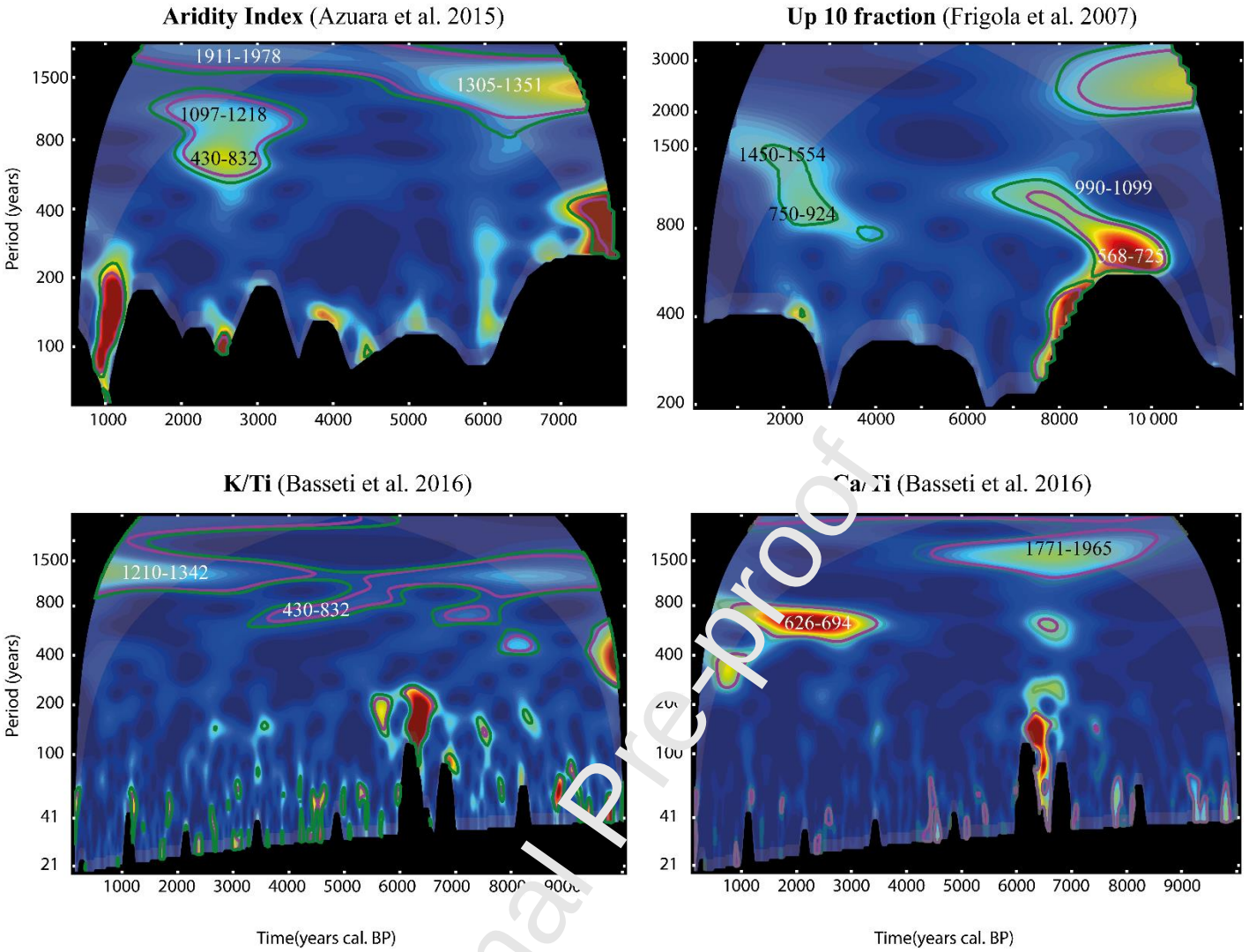

Figure 3 (part 1): Wavelet power spectra of the studied time series represented as scalograms. Colors indicate the amplitude of the wavelet power spectra, red being the highest amplitudes and blue the lowest. The purple lines represent the 95% confidence level, the green lines the 90% confidence level. The lateral grey shaded area represents the cone of influence and the lateral black areas the part of the time-scale plane excluded from the analysis because of the fixed length of integration for the smoothing of the sclalogram. The black and the grey shaded area at the bottom of each scalogram represent the SNEZ and its extension. Periodicities values of important cyclic periods including the age model errors (when available) are reported in black or white depending on the background color. Since the time series differ in length and resolution, scales are different from one spectrum to another.

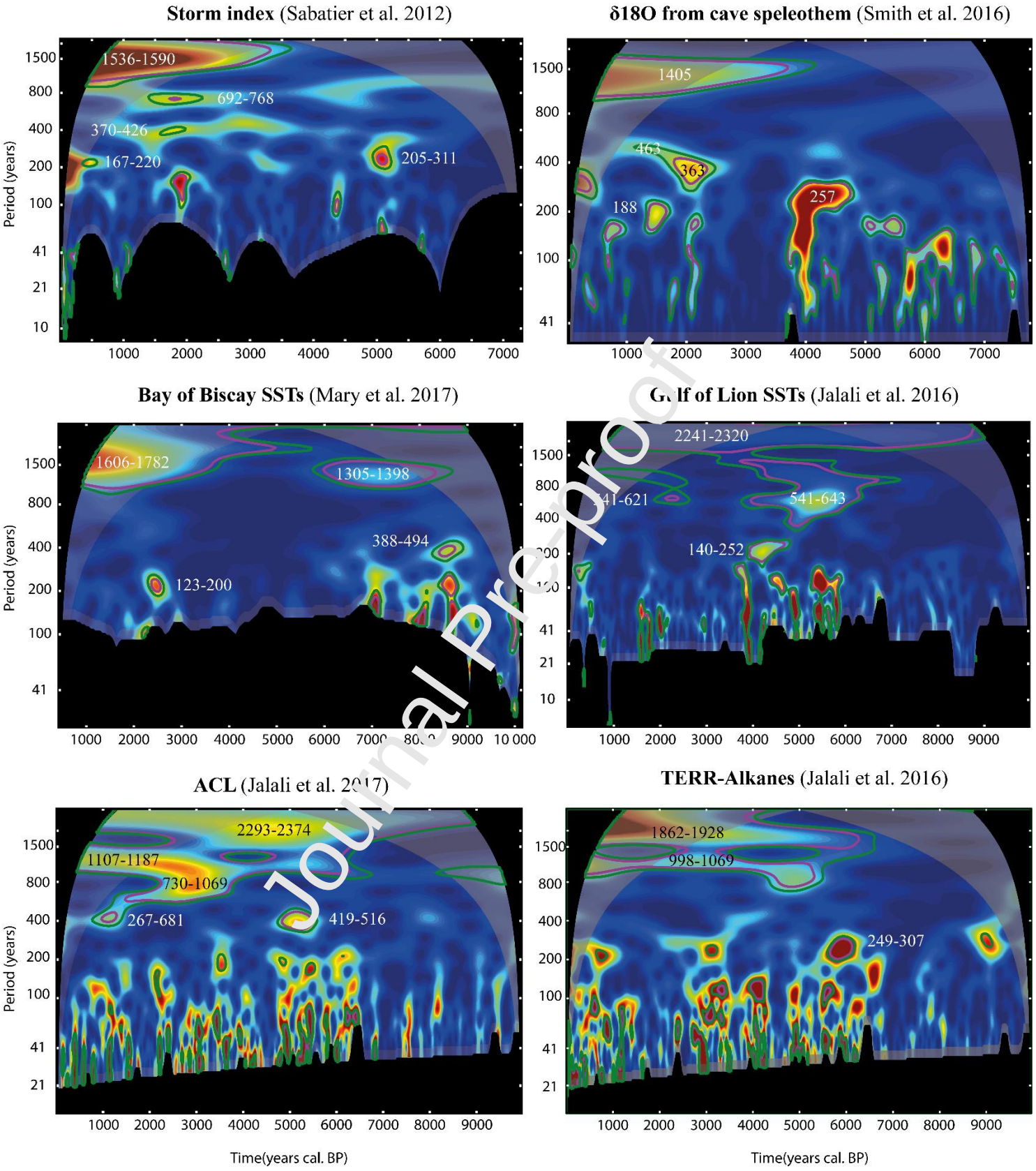

Figure 3 (part 2): see legend for Figure 3 (part 1).

Discussion

In this section, the frequency contents of each different paleoclimate proxy are compared to one another by direct comparison of the scalograms in order to better understand Holocene climate variability and its underlying mechanisms. To be considered as equivalent, cyclic periods from different time series need to have approximately the same period and to occur during the same time interval.

Oceanic forcing? The 1500 yrs cyclic period

SI, speleothem $\delta^{18}O$, Bay of Biscay SST and to a lesser extent Up10 fraction time series display a similar cyclic period of ~1400-1600 yrs after 5000 yrs cal BP (Figure 3). The comparison of these sequences filtered with a 1200-1700 yrs passband filter highlights time intervals of high (or low) storm activity in the Gulf of Lions that correspond to lower (or higher) precipitation in northwestern Spain and cooler (or warmer) SSTs in the Bay of Biscay since 5000 yrs cal BP (Figure 4). The time series are slightly off-set from each other (100-150), but these discrepancies are consistent with the order of magnitude of the age models' uncertainties (158.36 yrs).

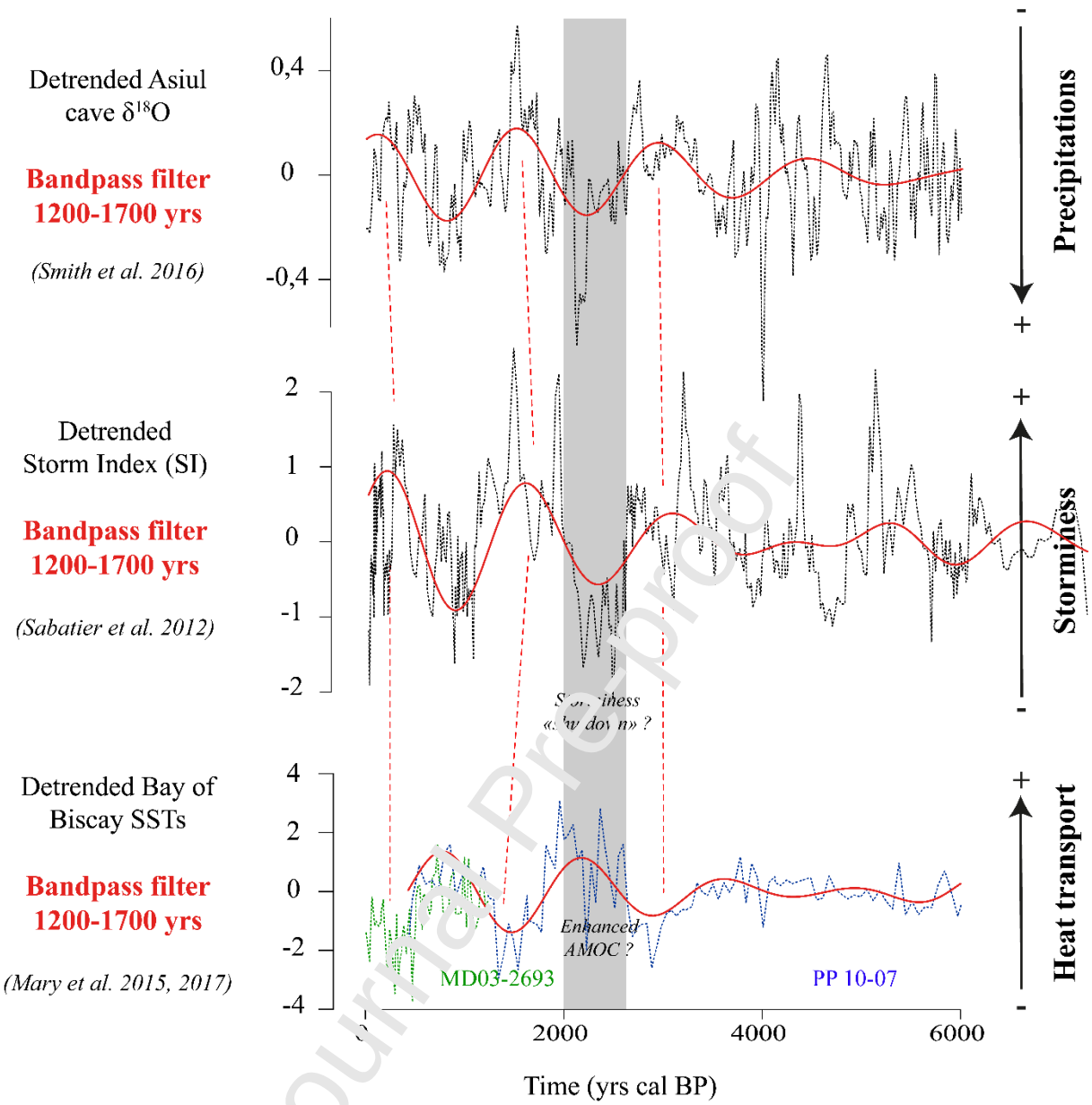

Figure 4: Comparison of the Asiul Cave speleothem $\delta^{18}O$, the Palavas Storm Index (SI) and the Bay of Biscay SSTs filtered with a 1200-1700 yrs bandpass filter to highlight variations linked to the ~1500 yrs cycles. The Bay of Biscay SSTs record from the PP 10-07 core (dashed blue curve, Mary et al. 2017) studied in this article is completed here with the SSTs record from the MD03-2693 core (dashed green curve, Mary et al. 2015) to show the important decrease in Bay of Biscay SSTs at the last part of the sequence. The shaded grey box highlights an event of enhanced AMOC revealed by the major increase in SSTs which probably resulted in a "storminess shutdown" in the Gulf of Lions.

Such ~1500 oscillations were first characterized by Bond et al. (2001) within stacked Ice Rafted Debris (IRD) records from the north Atlantic. Nevertheless, their gradual appearance during the second part of the Holocene and thus their non-stationarity, was first described by Debret et al. (2007) in several North Atlantic climate proxies including Bond's stacked IRD time series. Based on the predominance of this pattern in proxies specifically recording water mass activity in the Atlantic, Debret et al. (2007, 2009)

assumed that this variability reflected changes in the Atlantic thermohaline circulation. The detection of a similar cyclic period in the Bay of Biscay SSTs, which depend on the dynamics of Atlantic gyres, supports this hypothesis and further implies that these changes affect both deep and surface Atlantic waters. On the other hand, this ~1500 yrs variability is also evidenced in proxies relating to mid-latitude atmospheric circulation. Indeed, such cycles are also recorded in a storminess record from north-western Europe (Sorrel et al 2012) in phase with the high storm activity periods registered in the Gulf of Lions (Sabatier et al. 2012). Moreover, the speleothem $\delta^{18}O$ from northwestern Spain, which also displays these cycles, is related to advection of Atlantic low-pressure systems over the Iberian Peninsula. Thus, if internal fluctuations of the Atlantic thermohaline circulation are actually responsible for these late Holocene ~1500 years cyclic period, what mechanism might explain the fact that this frequency pattern also affects past atmosphere dynamics?

Experiments using ocean/atmosphere coupled models show an influence of the Atlantic Meridional Overturning Circulation (AMOC) on Atlantic storm track strength and position during winter time (Brayshaw et al. 2009, Woolings et al. 2012, Harvey et al. 2015). The Atlantic storm track is an area where depressions form preferentially and travel down the prevailing winds. Its strength corresponds to the number and the importance of the lows formed during a given period and is quantified using the variance of the Mean Sea Level Pressure (MSLP). In the models, AMOC weakening causes a strengthening of the storm track which spreads eastwards over northern Europe (Figure7). The weaker heat transport from the tropics toward the pole, because of the AMOC slowdown, induces cooler SSTs in the North Atlantic and increases sea ice extent in the Arctic. The resulting increase in the mid-latitude temperature gradient causes an increase in baroclinicity and thus cyclogenesis (Brayshaw et al. 2009, Woolings et al. 2012, Harvey et al. 2015). This mechanism would explain why a periodic weakening of the AMOC induces lower SSTs in the Bay of Biscay and causes an increase in storminess in northwestern Europe (Sorrel et al. 2012) by a direct increase in the number of depressions advected over this area.

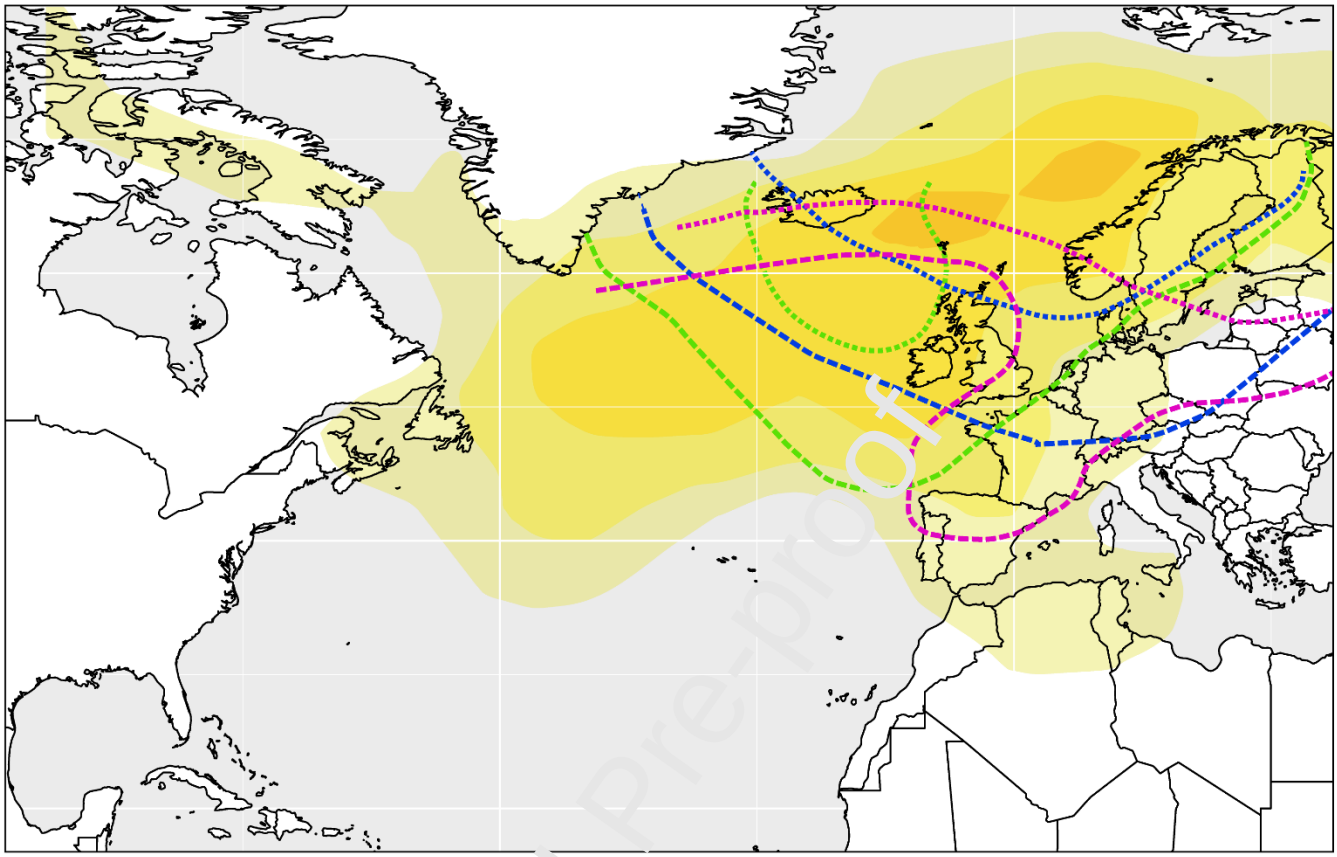

Figure 5: Comparison of the storm track response to AMOC reduction in experimental models (Woolings et al. 2012) and position of the lows during large scale circulation patterns which cause Mediterranean air masses to flow northwards over southern France, thereby perhaps leading to higher storm frequencies in the Gulf of Lions (Nuissier et al. 2011).

In the Gulf of Lions, heavy precipitation events and marine storms are both linked to the northward flow of warm, moist air masses from the Mediterranean, bringing humidity over areas of high relief and associated with very strong south-easterly to south-westerly winds (>40 $m.s^{-1}$) in the case of marine storms (Sabatier et al. 2008). Nuissier et al. (2011) identified the different Large-Scale Circulation patterns (LSC) leading to such northward flows of Mediterranean air masses by analyzing

meteorological data for wintertime between 1960 and 2000. The 500 hPa heights describing the altitude pressure field of these LSCs are reported on the map showing the response of the Atlantic storm track to AMOC weakening (Figure 5). The area of enhanced storm track strength encompasses the location of the low-pressure systems which could induce storms in the Gulf of Lions. Therefore, repetitive weakening of the AMOC, which strengthens the Atlantic storm track, could also explain the 1500 yrs cyclic period evident in the Palavas SI. Finally, Brayshaw et al. (2009) highlight the fact that a weakening of the AMOC can cause a decrease in winter precipitation over all of Western Europe, including the western Mediterranean area. Indeed, the SST reduction over the North Atlantic reduces the saturation water vapor pressure. Thus, despite the stronger zonal flow, the air masses from the Atlantic advected over Western Europe are cooler and drier. Since the speleothem $\delta^{18}O$ from northwestern Spain probably records winter precipitation in a region that is very sensitive to Atlantic influences (Smith et al. 2016), it reveals that the high storm activity periods are associated with lower precipitation in the northern Iberian Peninsula.

All of this evidence is consistent with several repetitive weakening of the AMOC during the latter part of the Holocene. Such variations are consistent with the well-known Bond events evident in North Atlantic IRD records (Bond et al. 2001). Sgubin et al. (2017) highlight that an important proportion (45.5%) of global climate models, which reproduce more accurately the structure of the North Atlantic Ocean, are predicting an imminent local collapse of the deep ocean convection in the Labrador Sea linked to the ongoing climate change. This possible interruption of deep-water formation could be similar to periodic weakening of the AMOC. Therefore, understanding the cause and the mechanism of such millennial scale climate variability appears crucial to improving our ability to predict the future climate.

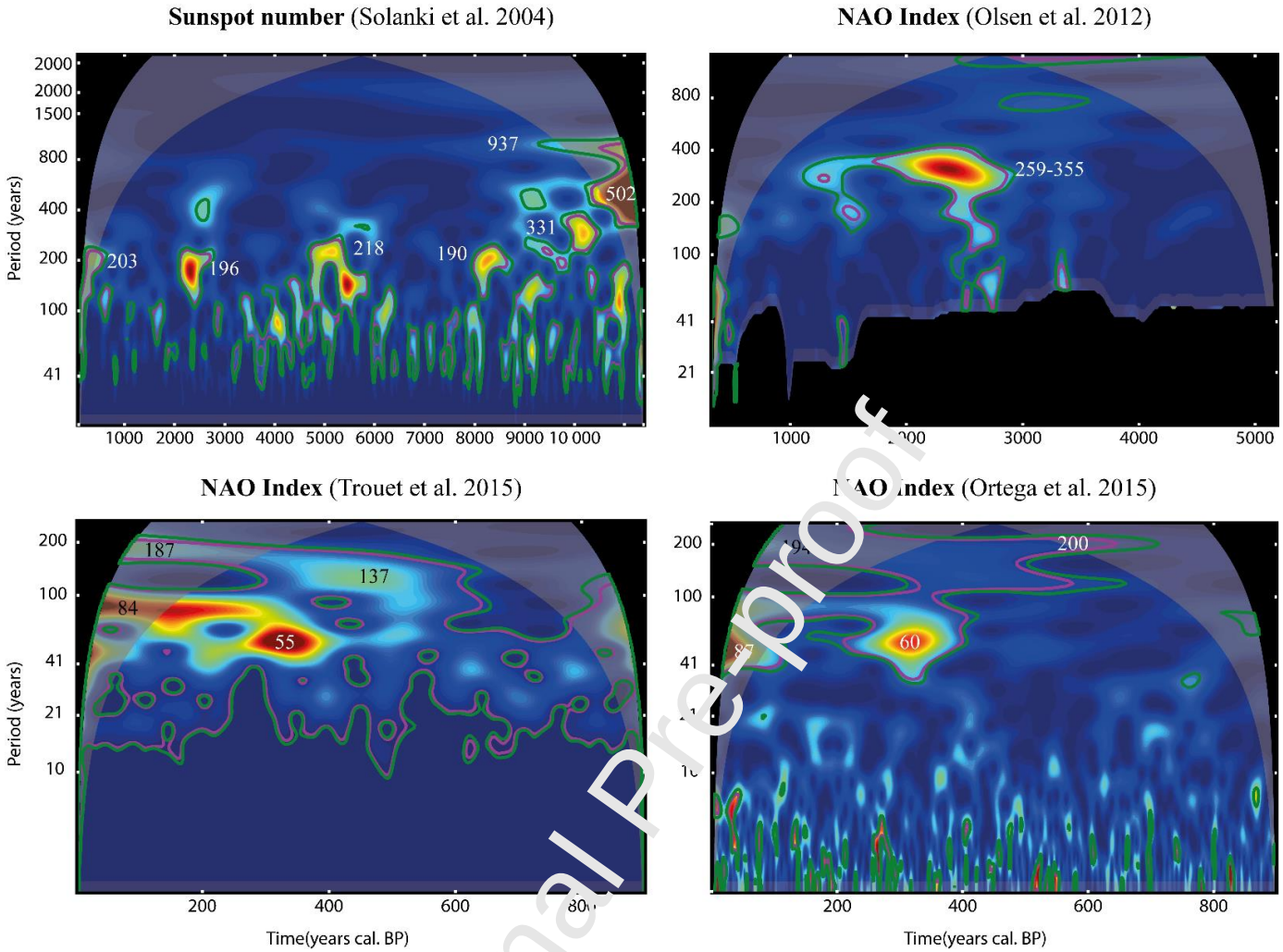

Figure 6: Wavelet power spectra of sunspot number record (Solanki et al. 2004) and NAO index records (Olsen et al. 2012, Trouet et al. 2015 and Ortega et al. 2015)

The two short cyclic periods of about ~200 yrs displayed in the SI time series (Figure 3) look similar to the 210 yrs so called De Vries cycles evidenced in solar activity proxies (Figure 6) (Stuiver and Braziunas 1989, Debret et al. 2007, Ma 2007, Debret et al. 2009, Steinhilber et al. 2012, Usokin et al. 2016). The influence of the centennial scale solar variability on Mediterranean storm frequency is further supported by a ~270 yrs periodicity found within a storminess record spanning the last 3000 yrs from the Bagnas pond, located about 40 km from Palavas, (Degeai et al. 2016).

Several studies conducted in Europe and in the Mediterranean also provide evidence for increases in precipitation and flood frequencies related to centennial scale solar variability (Wirth et al. 2013, Czymzik et al. 2016, Sabatier et al. 2017, Zielhofer et al. 2017). Results suggest that centennial scale changes in solar irradiance strongly affect atmospheric circulation in the European Atlantic sector inducing NAO-like variability (Raible et al. 2007, Martin-Puertas et al. 2012). To test if the 210 yrs solar cyclic periods could have induced changes in Gulf of Lions storminess through NAO-like atmospheric variability, the high-frequency content of SI and SN time series are compared with the

wavelet power spectra of three NAO Index records (Trouet et al. 2009, Olsen et al. 2012, Ortega et al. 2015). The longer NAO index record (Olsen et al. 2012) was reanalyzed to take into account age-model uncertainties. The variability of SI, SN and NAO time series within the 150-300 yrs bandwidth was compared (Figure 7).

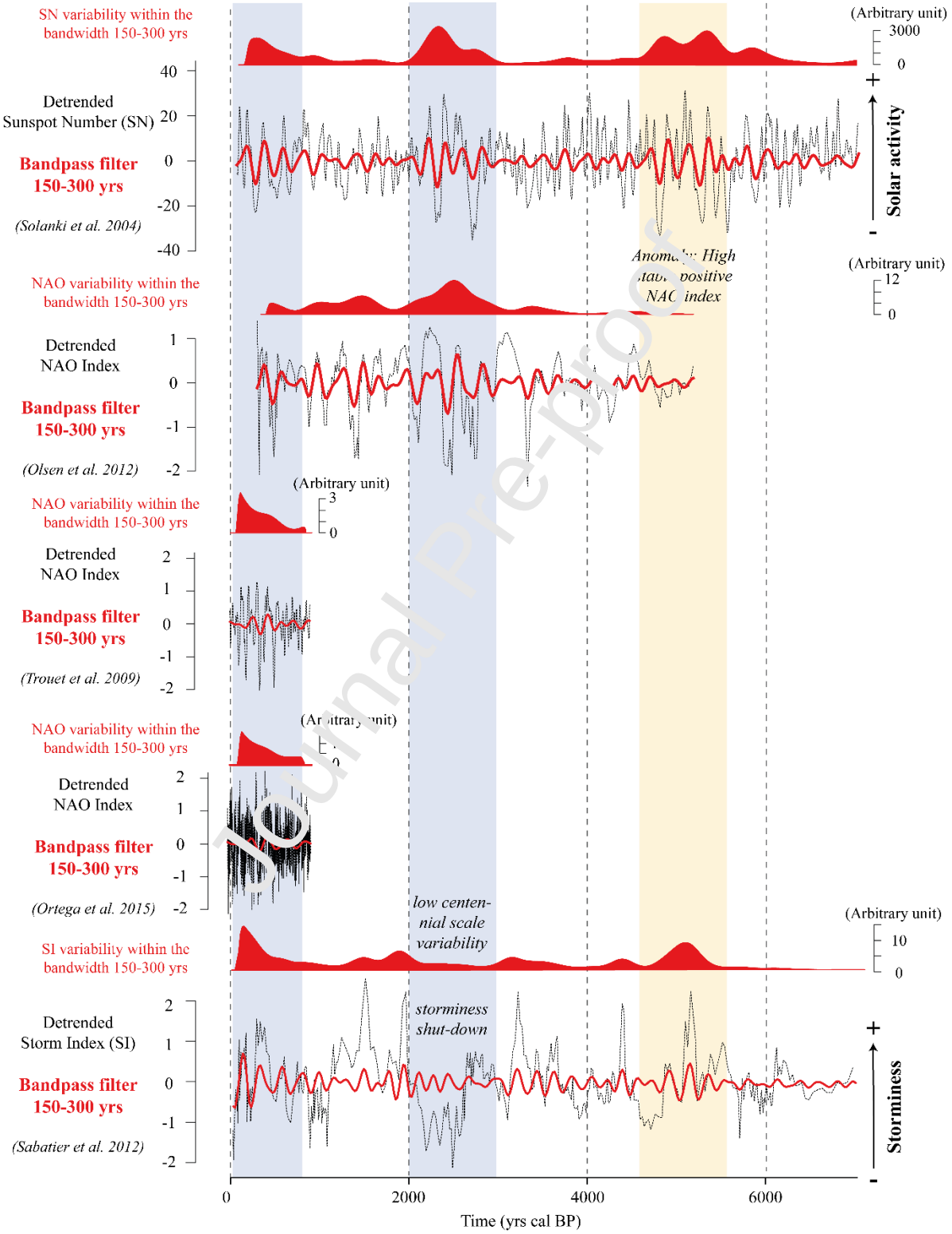

Figure 7: Comparison of the Sunspot number, the NAO indexes and the Palavas Storm Index (SI) filtered with a 150-300 yrs bandpass filter to highlight variations linked to the De Vries cycles. The filled red

curves correspond to the variability within the bandwidth 150-300 yrs obtained by summing the wavelet power over several scales. The shaded blue boxes highlight time intervals characterized by concomitant high solar and NAO index variability within the bandwidth 150-300 yrs. The shaded orange box highlights a time interval characterized by concomitant high solar and storminess variability without NAO index variability within the bandwidth 150-300 yrs.

This reanalysis of Olsen's NAO index reconstruction highlights a major significant cyclic period of 259-355 yrs between 3000 and 2000 yrs cal BP (Figure 12). Originally, this cyclic period was published as a 300 yrs cyclic period (Olsen et al. 2012). Thus, it was difficult to make the link with the 210 years De Vries variability. Our reanalysis indicate that this cyclic period could fit with the ~200 yrs cylic period evident within the SN time series during the same time interval (Figure 6).

On the one hand, the SN time series displays three periods of higher variability within the 150-300 yrs bandwidth. The first period of high centennial scale solar variability is located between ~850 yrs cal BP and the present. This period also corresponds to a period of high NAO variability and high storminess variability in the Gulf of Lions within the 150-300 yrs bandwidth (Figure 7). This concomitance of higher centennial scale variability in the solar activity, NAO and storminess proxies strongly supports the hypothesis that solar variability influences the north-western Mediterranean storm frequency through modifications of the atmospheric circulation. On the other hand, the second period of high centennial scale solar variability between 3000 and 2000 yrs cal BP again corresponds to a period of high NAO variability but is associated with very low centennial scale storminess variability. Nevertheless, this period corresponds to one of the long-term decreases in storminess previously discussed. Indeed, at this time, the Palavas SI drops dramatically while Bay of Biscay SSTs display an exceptional increase, just as the Mediterranean storminess was "shut-down" due to a very strong AMOC which caused a contraction of the Atlantic storm track toward the east (Figure 4). Therefore, this situation might represent a case of millennial scale internal variability bypassing the centennial scale external variability. Finally, around 5250 yrs cal BP, both SI and SN time series display significant variability within the 150-300 yrs bandwidth, just when the NAO variability is very low with NAO index values remaining very high (Figure 7). However, since Olsen's NAO index reconstruction (Olsen et al. 2012) is based on only one proxy, and for now no other NAO reconstructions exist for this period, these NAO index values must be considered with caution. Indeed, Ortega et al. (2015) point out the necessity of multi-proxy studies to improve the reliability of NAO index reconstructions. They also highlight the unrealistic character of long and persistent positive NAO periods. Therefore, given these elements, this discrepancy between the NAO index variability and the solar and storminess variabilities around 5250 yrs cal BP does not invalidate the hypothesis of solar induced storminess changes through changes in the atmospheric circulation. However, further work is necessary to characterize the middle Holocene climate and the mechanisms of variability during this period.

ENSO influences?

The major changes in SST and atmospheric surface pressures characterizing the ENSO variability in the tropical Pacific, also affect climate variability at higher latitudes in very remote parts of the globe (Brönnimann et al. 2007). Many studies relying on instrumental data (Loon and Madden, 1981; Fraedrich 1990, 1994; Fraedrich and Müller,1992; May and Bengtsson, 1998; Mariotti et al. 2002; Xoplaki 2002 ; Gouirand and Moron, 2003; Moron and Gouirand, 2003; Muñoz-Diaz and Rodrigo, 2005; Mariotti et al. 2005; Pozo-Vazquez et al. 2005) and on experiments based on Ocean-atmosphere coupled models (Raible et al. 2001, 2004; Deser et al. 2006; Brönnimann et al. 2007) support a non-stationary but significant influence of ENSO variability on Western Europe including the Western Mediterranean. Such remote influence of the pacific area on the European climate is further supported by results from climate reconstruction over the past 245 years (Rimbu et al. 2003) and even the last 500 yrs (Mann et al. 2000; Brönnimann et al. et al. 2007). Therefore, in this section our attention focuses on the potential influence of ENSO variability on the northwestern Mediterranean climate throughout the mid- to late Holocene.

To address this issue, the frequency content of the western Mediterranean paleoclimate sequences was compared with the frequency content of a high-resolution ENSO variability record from the Ecuadorian Andes spanning the Holocene (Moy et al. 2002) and with an ITCZ position record within the Cariaco Basin in the tropical Atlantic (Haug et al. 2001) (Figure 8). Considering that the tropical Atlantic is influenced by the ENSO variability (Ruiz-Barradas et al. 2003; Wang et al. 2004) and thus could be an intermediary between the eastern Pacific and the south-western Europe climate variability (Brönnimann et al. 2007), the ICTZ record from the Caribbean is complementary to the ENSO record from the Andes.

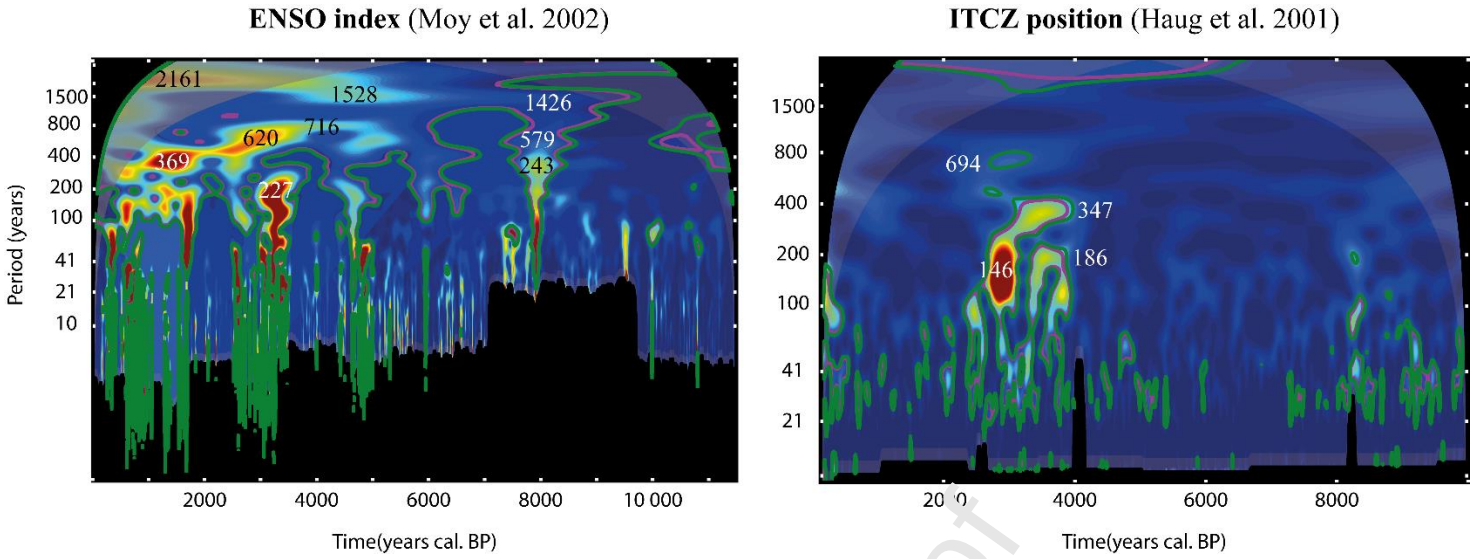

Figure 8: Wavelet power spectra of the ENSO variability time series from Pallcacocha in the Ecuadorian Andes (Moy et al. 2002) and the ITCZ position in the Cariaco basin (Haug et al. 2001). See legend Figure 3.

The ENSO variability and to a lesser extent the ITCZ record show some interesting cyclic periods which might correspond to unattributed cyclic periods recorded in our Mediterranean and Atlantic proxy time series (Figure 8). The ENSO ~716 to 6200 yrs cyclic period between 5000 and 2000 yrs cal BP (Figure 8) which seems also recorded in the ITCZ record (694 yrs cyclic period between 3000 and 2000 yrs cal BP) remind the following cyclic periods in the Mediterranean and Atlantic sequences:

i. 730-1069 yrs between 4000 and 2000 yrs cal BP (ACL)

ii. 692-768 yrs between 3000 and 1900 yrs cal BP (SI)

iii. 430-832 yrs between 3000 and 2000 yrs cal BP (AI)

iv. 626-694 yrs between 2000 and 1000 yrs cal BP (Ca/Ti)

v. 541-621 yrs around 2000 yrs cal BP (Gulf of Lion SST)

In a similar way, the ENSO ~1426 to 1528 yrs cyclic period between 9000-5000 yrs cal BP (Figure 8) remind the cyclic periods of:

i. 1300-1651 yrs between 7500 and 5000 yrs cal BP (AI)

ii. 1300 -1400 yrs between 9000 and 5000 yrs cal BP (K/Ti)

iii. 1300-1398 yrs between 9000 and 5500 yrs (Bay of Biscay SST)

Finally, the ENSO ~369 yrs cyclic period 2000 and 1000 yrs cal BP remind the cyclic periods of:

i. 267-681 yrs around 1000 yrs cal BP (ACL)

ii. 370-426 yrs between 1500 and 2000 yrs cal BP (SI)

iii. ~463 yrs between 2000 and 1000 yrs cal BP (Asiul cave speleothem $\delta^{18}O$)

Thus, even if the influence of age models' errors uncertainties on the scalograms of these two tropical records were not quantified, the ENSO climate variability seems to be detectable in Mediterranean and Altantic paleoclimatic proxies, especially in ACL, AI, Ca/TI and Bay of Biscay SST records for which these cyclic periods represent major features.

These shared cyclic periods are consistent with an influence of the ENSO variability on western Mediterranean precipitation through the Atlantic (Brönnimann et al. 2007). Indeed, Bay of Biscay SSTs record past dynamics of the Atlantic gyres (Mary et al. 2017), AI and ACL are indices of aridity in the western Mediterranean, Ca/Ti is a proxy influenced by precipitation in the Rhône watershed and SI in the Gulf of Lion can be linked to the NAO variability (see previous paragraph). Models and instrumental data reanalysis show that such a connection is possible (Brönnimann et al. 2007). One of the mechanisms that has been most studied involves a downstream propagation of ENSO impact along a North-Pacific/North-Atlantic connection during boreal winters. The season-averaged mid-latitude atmospheric circulation can be broken down into two components: (i) the zonal mean flow and (ii) asymmetric features arising from irregularities of the earth's surface (mountains, continent-ocean contrast, sea surface temperature asymmetries, etc.) referred to as stationary waves (Held et al. 2002, Nigam and DeWeaver, 2003). During boreal winters, when the amplitude of these stationary waves is maximal in the Northern Hemisphere (Nigam and DeWeaver, 2003), the ENSO events may change their structure by disrupting Hadley's circulation (Brönnimann et al. 2007). Such a change of the quasi-stationary wave over the north Atlantic can impact, among other things, on the cyclogenesis of this area, the Icelandic low and NAO variability (e.g. Honda et al. 2001, Raible 2001, Moron and Gouirand 2003). Another mechanism involves a connection between the tropical Pacific and the North-Atlantic through the tropical Atlantic during spring (Brönnimann et al. 2007). Indeed, ENSO variability could affect the Azores high and hence the NAO, by disrupting Atlantic Hadley circulation (Cassou and Terray, 2001). ENSO could also affect European climate through a downward propagation of stratospheric anomalies (e.g. Randel, 2004; Manzini et al. 2006). Finally, the shared cyclic period (670 yrs) between ENSO and Bay of Biscay SSTs could be the result of a possible reciprocal interaction between tropical Atlantic SSTs and ENSO. Indeed, several studies have highlighted that such a teleconnection can affect the mid- to high latitude North Atlantic thermohaline circulation (Chiang and Sobel, 2002; Svendsen et al. 2014 and reference therein).

Although further research is needed to better understand the relative importance of the different Pacific/Atlantic coupling mechanisms, and the link between ENSO and European climate at the decadal and multidecadal scale (Brönnimann et al. 2007), all of the studies mentioned above render the ENSO

influence a credible hypothesis to explain the similarities in frequency content between records in the north-western Mediterranean and those in the eastern Pacific and the tropical Atlantic. However, the shared cyclicities between the tropical and the western Mediterranean time series could also arise from an as yet unidentified independent climate forcing, which might influence both ENSO and the Mediterranean variability without implying any direct link between them. Thus, further investigation is needed to accurately address the question of the potential influence of ENSO variability on the north-western Mediterranean climate throughout the Holocene. However, a review of the frequency content of a full set of paleoclimatic time series from the tropical areas in order to investigate this issue is a huge task beyond the scope of this article.

Conclusion

Ten paleoclimate time series from the Gulf of Lions and the surrounding areas, together with NAO index, ENSO variability and ICTZ position time series, were compared in the frequency domain using wavelet analysis. Since direct comparison of all of their oscillations is not informative, the comparison of their frequency content is used to discuss directly the forcing and mechanism underlying Mediterranean climate variability. Indeed, three main groups of shared cyclic periods may be defined on the basis of the results of our analysis: (i) an Atlantic cyclic period of ~1500 yrs since 5000 yrs cal BP, (ii) solar cyclic periods of 210 yrs displayed around 500 and 5000 yrs cal BP and (iii) tropical cyclic periods of 670, 1500 and 1900 yrs recorded respectively around 2500, 4000 and 6500 yrs cal BP. The Atlantic cyclic period of ~1500 yrs is probably related to repetitive fluctuations of the Atlantic thermohaline circulation which induces changes in the storm track extension and position, with impacts on both precipitation and storminess over a millennial scale. The centennial scale solar variability might induce a NAO-like variability of the atmospheric circulation influencing the storminess in Western Europe and in the western Mediterranean. Finally, the tropical features recorded in many climate proxies from the Gulf of Lions, might highlight the influence of the ENSO climate variability over the western Mediterranean.

Of course, further studies are needed to better characterize and understand Mediterranean climate variability during the Holocene period. The link between the tropical latitudes and the Mediterranean Basin needs to be better characterized. Moreover, one might wonder to what extent the leading mechanisms of climatic change described here influence and control climatic variability in the Eastern Mediterranean, considering the east-west see-saw pattern described by Roberts et al. (2012). We might also ask whether the described patterns are valid in the southern Mediterranean realm, given the north-south paleohydrological contrast reported by Magny et al. (2013). Nevertheless, the results presented in this review article establish a state of the art for paleoclimate variability in the north-western Mediterranean area. This approach allows us to understand the "natural" millennial and centennial scale variability of the earth's climate system in this climatic change hot spot (Giorgi, 2006) Wavelet analysis

of paleoclimate time series can undoubtedly make a valuable contribution to studies on improving predictions of ongoing anthropogenic climate change.

Acknowledgements

This research was funded by MISTRALS/PALEOMEX meta-program, the CNRS and the French Museum of National History (MNHN). Paleoclimate time series were extracted from the PANGEA and the NOAA database and the work of the data contributors and the PANGEA and NOAA communities is gratefully acknowledged. None of the authors have conflicts of interest to declare.

Conflict of interests

All authors approve the publication of this work in Earth-Science Reviews and none of them have conflicts of interest to declare.

References

Alley, R.B., Mayewski, P.A., Sowers, T., Stuiver, M., Taylor, K.C., Clark, P.U., 1997. Holocene climatic instability: A prominent, widespread event 8200 yr ago. Geology 25, 483–486.

Anchukaitis, K.J., Tierney, J.E., 2013. Identifying coherent spatiotemporal modes in time-uncertain proxy paleoclimate records. Climate Dynamics 41, 1291–1306. doi:10.1007/s00382-012-1483-0

Azuara, J., Combourieu-Nebout, N., Lebreton, V., Mazier, F., Müller, S.D., Dezileau, L., 2015. Late Holocene vegetation changes in relation with climate fluctuations and human activity in Languedoc (southern France). Climate of the Past 11, 1769–1784. doi:10.5194/cp-11-1769-2015

Azuara, J., Lebreton, V., Peyron, O., Mazier, F., Combourieu-Nebout, N., 2018. The Holocene history of low altitude Mediterranean Fagus sylvatica forests in southern France. Journal of Vegetation Science 29, 438–449.

Babu, P., Stoica, P., 2010. Spectral analysis of nonuniformly sampled data–a review. Digital Signal Processing 20, 359–378.

Bar-Matthews, M., Ayalon, A., 2011. Mid-Holocene climate variations revealed by high-resolution speleothem records from Soreq Cave, Israel and their correlation with cultural changes. The Holocene 21, 163–171. doi:10.1177/0959683610384165

Bassetti, M.-A., Berné, S., Sicre, M.-A., Dennielou, B., Alonso, Y., Buscail, R., Jalali, B., Hebert, B., Menniti, C., 2016. Holocene hydrological changes in the Rhône River (NW Mediterranean) as recorded in the marine mud belt. Climate of the Past 12, 1539–1553. doi:10.5194/cp-12-1539-2016

Billeaud, I., Tessier, B., Lesueur, P., 2009. Impacts of late Holocene rapid climate changes as recorded in a macrotidal coastal setting (Mont-Saint-Michel Bay, France). Geology 37, 1031–1034.

Blaauw, M., 2010. Methods and code for 'classical' age-modelling of radiocarbon sequences. quaternary geochronology 5, 512–518.

Bond, G., 2001. Persistent Solar Influence on North Atlantic Climate During the Holocene. Science 294, 2130–2136. doi:10.1126/science.1065680

Bond, G., 1997. A Pervasive Millennial-Scale Cycle in North Atlantic Holocene and Glacial Climates. Science 278, 1257–1266. doi:10.1126/science.278.5341.1257

Brayshaw, D.J., Woollings, T., Vellinga, M., 2009. Tropical and Extratropical Responses of the North Atlantic Atmospheric Circulation to a Sustained Weakening of the MOC. Journal of Climate 22, 3146–3155. doi:10.1175/2008JCLI2594.1

Broecker, W.S., Sutherland, S., Peng, T.-H., 1997. Slowdown of Southern Ocean Deep Water Formation. J. Biochem 250, 99.

Brönnimann, S., Xoplaki, E., Casty, C., Pauling, A., Luterbacher, J., 2007. ENSO influence on Europe during the last centuries. Climate Dynamics 28, 181–197.

Bueh, C., Nakamura, H., 2007. Scandinavian pattern and its climatic impact. Quarterly Journal of the Royal Meteorological Society 133, 2117–2131.

Cassou, C., Terray, L., 2001. Dual influence of Atlantic and Pacific SST anomalies on the North Atlantic/Europe winter climate. Geophysical research letters 28, 3195–3198.

Cassou, C., Terray, L., Phillips, A.S., 2005. Tropical Atlantic influence on European heat waves. Journal of climate 18, 2805–2811.

Chiang, J.C., Sobel, A.H., 2002. Tropical tropospheric temperature variations caused by ENSO and their influence on the remote tropical climate. Journal of climate 15, 2616–2631.

Combourieu Nebout, N., Peyron, O., Dormoy, I., Desprat, S., Beaudouin, C., Kotthoff, U., Marret, F., 2009. Rapid climatic variability in the west Mediterranean during the last 25 000 years from high resolution pollen data. Climate of the Past 5, 503–521.

Conte, M., Giuffrida, A., Tedesco, S., 1989. Mediterranean Oscillation: Impact on Precipitation and Hydrology in Italy, in: Conference on Climate and Water.

Conte, M.H., Sicre, M.-A., Rühlemann, C., Weber, J.C., Schulte, S., Schulz-Bull, D., Blanz, T., 2006. Global temperature calibration of the alkenone unsaturation index (UK′ 37) in surface waters and comparison with surface sediments. Geochemistry, Geophysics, Geosystems 7.

Costas, S., Naughton, F., Goble, R., Renssen, H., 2016. Windiness spells in SW Europe since the last glacial maximum. Earth and Planetary Science Letters 436, 82–92.

Czymzik, M., Muscheler, R., Brauer, A., 2016. Solar modulation of flood frequency in central Europe during spring and summer on interannual to multi-centennial timescales. Climate of the Past 12, 799–805.

Debret, M., Bout-Roumazeilles, V., Grousset, F., Desmet, M., McManus, J.F., Massei, N., Sebag, D., Petit, J.-R., Copard, Y., Trentesaux, A., 2007. The origin of the 1500-year climate cycles in Holocene North-Atlantic records. Climate of the Past Discussions 3, 679–692.

Debret, M., Sebag, D., Crosta, X., Massei, N., Petit, J.-R., Chapron, E., Bout-Roumazeilles, V., 2009. Evidence from wavelet analysis for a mid-Holocene transition in global climate forcing. Quaternary Science Reviews 28, 2675–2688. doi:10.1016/j.quascirev.2009.06.005

Degeai, J.-P., Devillers, B., Dezileau, L., Oueslati, H., Bony, G., 2015. Major storm periods and climate forcing in the Western Mediterranean during the Late Holocene. Quaternary Science Reviews 129, 37–56. doi:10.1016/j.quascirev.2015.10.009

deMenocal, P., Ortiz, J., Guilderson, T., Adkins, J., Sarnthein, M., Baker, L., Yarusinsky, M., 2000. Abrupt onset and termination of the African Humid Period:: rapid climate responses to gradual insolation forcing. Quaternary science reviews 19, 347–361.

Deser, C., Capotondi, A., Saravanan, R., Phillips, A.S., 2006. Tropical Pacific and Atlantic climate variability in CCSM3. Journal of Climate 19, 2451–2481.

Dezileau, L., Bordelais, S., Condomines, M., Bouchette, F., Briqueu, L., 2005. Evolution des lagunes du Golfe d'Aigues-Mortes à partir de l'étude de carottes sédimentaires courtes (étude géochronologique, sédimentologique et géochimique des sédiments récents). Publications ASF, Paris 51, 91.

Dezileau, L., Pérez-Ruzafa, A., Blanchemanche, P., Degeai, J.-P., Raji, O., Martinez, P., Marcos, C., Von Grafenstein, U., 2016. Extreme storms during the last 6500 years from lagoonal sedimentary archives in the Mar Menor (SE Spain). Climate of the Past 12, 1389–1400. doi:10.5194/cp-12-1389-2016

Dezileau, L., Sabatier, P., Blanchemanche, P., Joly, B., Swingedouw, D., Cassou, C., Castaings, J., Martinez, P., Von Grafenstein, U., 2011. Intense storm activity during the Little Ice Age on the French Mediterranean coast. Palaeogeography, Palaeoclimatology, Palaeoecology 299, 289–297. doi:10.1016/j.palaeo.2010.11.009

Dima, M., Lohmann, G., 2009. Conceptual model for millennial climate variability: a possible combined solar-thermohaline circulation origin for the ~1,500-year cycle. Climate Dynamics 32, 301–311. doi:10.1007/s00382-008-0471-x

Farge, M., 1992. Wavelet transforms and their applications to turbulence. Annual review of fluid mechanics 24, 395–458.

Fletcher, W.J., Debret, M., Goñi, M.F.S., 2013. Mid-Holocene emergence of a low-frequency millennial oscillation in western Mediterranean climate: Implications for past dynamics of the North Atlantic atmospheric westerlies. The Holocene 23, 153–166.

Foster, G., 1996. Wavelets for period analysis of unevenly sampled time series. The Astronomical Journal 112, 1709.

Fraedrich, K., 1994. An ENSO impact on Europe? Tellus A 46, 541–552.

Fraedrich, K., 1990. European grosswetter during the warm and cold extremes of the El Niñco/Southern Oscillation. International Journal of Climatology 10, 21–31.

Fraedrich, K., Müller, K., 1992. Climate anomalies in Europe associated with ENSO extremes. International Journal of Climatology 12, 25–31.

Frigola, J., Moreno, A., Cacho, I., Canals, M., Sierro, F.J., Flores, J.A., Grimalt, J.O., Hodell, D.A., Curtis, J.H., 2007. Holocene climate variability in the western Mediterranean region from a deepwater sediment record: HOLOCENE CLIMATE VARIABILITY. Paleoceanography 22. doi:10.1029/2006PA001307

Gagosian, R.B., Peltzer, E.T., 1986. The importance of atmospheric input of terrestrial organic material to deep sea sediments. Organic Geochemistry 10, 661–669.

Giraudi, C., 2005. Middle to Late Holocene glacial variations, periglacial processes and alluvial sedimentation on the higher Apennine massifs (Italy). Quaternary Research 64, 176–184.

Giraudi, C., Magny, M., Zanchetta, G., Drysdale, R.N., 2011. The Holocene climatic evolution of Mediterranean Italy: A review of the continental geological data. The Holocene 21, 105–115.

Gouirand, I., Moron, V., 2003. Variability of the impact of El Niño–southern oscillation on sea-level pressure anomalies over the North Atlantic in January to March (1874–1996). International journal of climatology 23, 1549–1566.

GROUP, M., 1970. Observation of formation of deep water in the Mediterranean Sea, 1969.

Harvey, B.J., Shaffrey, L.C., Woollings, T.J., 2015. Deconstructing the climate change response of the Northern Hemisphere wintertime storm tracks. Climate dynamics 45, 2847–2860.

Haug, G.H., Hughen, K.A., Sigman, D.M., Peterson, L.C., Röhl, U., 2001. Southward migration of the intertropical convergence zone through the Holocene. Science 293, 1304–1308.

Held, I.M., Ting, M., Wang, H., 2002. Northern winter stationary waves: Theory and modeling. Journal of climate 15, 2125–2144.

Honda, M., Nakamura, H., Ukita, J., Kousaka, I., Takeuchi, K., 2001. Interannual seesaw between the Aleutian and Icelandic lows. Part I: Seasonal dependence and life cycle. Journal of climate 14, 1029–1042.

Hurrell, J.W., Kushnir, Y., Ottersen, G., Visbeck, M., 2003. An overview of the North Atlantic oscillation. The North Atlantic Oscillation: climatic significance and environmental impact 134, 1–35.

Jalali, B., Sicre, M.-A., Bassetti, M.-A., Kallel, N., 2016. Holocene climate variability in the north-western Mediterranean Sea (gulf of lions). Climate of the Past Discussions 91–120.

Jalali, B., Sicre, M.-A., Kallel, N., Azuara, J., Combourieu-Nebout, N., Bassetti, M.-A., Klein, V., 2017. High-resolution Holocene climate and hydrological variability from two major Mediterranean deltas (Nile and Rhone). The Holocene 0959683616683258.

Jalut, G., Dedoubat, J.J., Fontugne, M., Otto, T., 2009. Holocene circum-Mediterranean vegetation changes: Climate forcing and human impact. Quaternary International 200, 4–18. doi:10.1016/j.quaint.2008.03.012

Jaouadi, S., Lebreton, V., Bout-Roumazeilles, V., Siani, G., Lakhdar, R., Boussoffara, R., Dezileau, L., Kallel, N., Mannai-Tayech, B., Combourieu-Nebout, N., 2016. Environmental changes, climate and anthropogenic impact in south-east Tunisia during the last 8 kyr. Climate of the Past 12, 1339–1359. doi:10.5194/cp-12-1339-2016

Jiménez-Moreno, G., Rodríguez-Ramírez, A., Pérez-Asensio, J.N., Carrión, J.S., López-Sáez, J.A., Villarías-Robles, J.J., Celestino-Pérez, S., Cerrillo-Cuenca, E., León, Á., Contreras, C., 2015. Impact of late-Holocene aridification trend, climate variability and geodynamic control on the environment from a coastal area in SW Spain. The Holocene 25, 607–617.

Joly, B., Girardot, N., Roulet, B., Labadie, C., 2012. Experimental Daily Forecasts of Northern Atlantic Weather Regimes and Heavy Precipitating Events (HPEs) over Southern France with the Meteo France Global Ensemble System PEARP.

Jongma, J.I., Prange, M., Renssen, H., Schulz, M., 2007. Amplification of Holocene multicentennial climate forcing by mode transitions in North Atlantic overturning circulation: HOLOCENE MULTICENTENNIAL CLIMATE FORCING. Geophysical Research Letters 34. doi:10.1029/2007GL030642

Lebeaupin Brossier, C., Drobinski, P., 2009. Numerical high-resolution air-sea coupling over the Gulf of Lions during two tramontane/mistral events. Journal of Geophysical Research: Atmospheres 114.

Lenoir, G., Crucifix, M., 2018a. A general theory on frequency and time–frequency analysis of irregularly sampled time series based on projection methods–Part 1: Frequency analysis. Nonlinear Processes in Geophysics 25, 145.

Lenoir, G., Crucifix, M., 2018b. A general theory on frequency and time–frequency analysis of irregularly sampled time series based on projection methods–Part 2: Extension to time–frequency analysis. Nonlinear Processes in Geophysics 25.

Lionello, P., Trigo, I.F., Gil, V., Liberato, M.L.R., Nissen, K.M., Pinto, J.G., Raible, C.C., Reale, M., Tanzarella, A., Trigo, R.M., Ulbrich, S., Ulbrich, U., 2016. Objective climatology of cyclones in the Mediterranean region: a consensus view among methods with different system identification and tracking criteria. Tellus A: Dynamic Meteorology and Oceanography 68, 29391. doi:10.3402/tellusa.v68.29391

Loon, H., Madden, R.A., 1981. The Southern Oscillation. Part I: Global associations with pressure and temperature in northern winter. Monthly Weather Review 109, 1150–1162.

Ludwig, W., Dumont, E., Meybeck, M., Heussner, S., 2009. River discharges of water and nutrients to the Mediterranean and Black Sea: major drivers for ecosystem changes during past and future decades? Progress in Oceanography 80, 199–217.

Magny, M., Bégeot, C., Guiot, J., Peyron, O., 2003. Contrasting patterns of hydrological changes in Europe in response to Holocene climate cooling phases. Quaternary Science Reviews 22, 1589–1596. doi:10.1016/S0277-3791(03)00131-8

Magny, M., Combourieu-Nebout, N., De Beaulieu, J.L., Bout-Roumazeilles, V., Colombaroli, D., Desprat, S., Francke, A., Joannin, S., Peyron, O., Revel, M., 2013. North-south palaeohydrological contrasts in the central Mediterranean during the Holocene: tentative synthesis and working hypotheses. Climate of the Past Discussions 9, 1901–1967.

Magny, M., de Beaulieu, J.-L., Drescher-Schneider, R., Vannière, B., Walter-Simonnet, A.-V., Miras, Y., Millet, L., Bossuet, G., Peyron, O., Brugiapaglia, E., Leroux, A., 2007. Holocene climate changes in the central Mediterranean as recorded by lake-level fluctuations at Lake Accesa (Tuscany, Italy). Quaternary Science Reviews 26, 1736–1758. doi:10.1016/j.quascirev.2007.04.014

Magny, M., Miramont, C., Sivan, O., 2002. Assessment of the impact of climate and anthropogenic factors on Holocene Mediterranean vegetation in Europe on the basis of palaeohydrological records. Palaeogeography, Palaeoclimatology, Palaeoecology 186, 47–59.

Magny, M., Peyron, O., Sadori, L., Ortu, E., Zanchetta, G., Vannière, B., Tinner, W., 2012. Contrasting patterns of precipitation seasonality during the Holocene in the south- and north-central Mediterranean. Journal of Quaternary Science 27, 290–296. doi:10.1002/jqs.1543

Mann, M.E., Bradley, R.S., Hughes, M.K., 2000. Long-term variability in the El Nino Southern Oscillation and associated teleconnections. Cambridge University Press, Cambridge, UK.

Manzini, E., Giorgetta, M.A., Esch, M., Kornblueh, L., Roeckner, E., 2006. The influence of sea surface temperatures on the northern winter stratosphere: Ensemble simulations with the MAECHAM5 model. Journal of climate 19, 3863–3881.

Mariotti, A., Ballabrera-Poy, J., Zeng, N., 2005. Tropical influence on Euro-Asian autumn rainfall variability. Climate Dynamics 24, 511–521.

Mariotti, A., Zeng, N., Lau, K.-M., 2002. Euro-Mediterranean rainfall and ENSO—a seasonally varying relationship. Geophysical research letters 29.

Martin-Puertas, C., Matthes, K., Brauer, A., Muscheler, R., Hansen, F., Petrick, C., Aldahan, A., Possnert, G., van Geel, B., 2012. Regional atmospheric circulation shifts induced by a grand solar minimum. Nature Geoscience 5, 397–401. doi:10.1038/ngeo1460

Martin-Vide, J., Lopez-Bustins, J.-A., 2006. The western Mediterranean oscillation and rainfall in the Iberian Peninsula. International Journal of Climatology 26, 1455–1475.

Mary, Y., Eynaud, F., Colin, C., Rossignol, L., Brocheray, S., Mojtahid, M., Garcia, J., Peral, M., Howa, H., Zaragosi, S., Cremer, M., 2017. Changes in Holocene meridional circulation and poleward Atlantic flow: the Bay of Biscay as a nodal point. Climate of the Past 13, 201–216. doi:10.5194/cp-13-201-2017

Mathias, A., Grond, F., Guardans, R., Seese, D., Canela, M., Diebner, H.H., Baiocchi, G., 2004. Algorithms for spectral analysis of irregularly sampled time series. Journal of Statistical Software 11, 1–30.

May, W., Bengtsson, L., 1998. The signature of ENSO in the Northern Hemisphere midlatitude seasonal mean flow and high-frequency intraseasonal variability. Meteorology and Atmospheric Physics 69, 81–100.

Mayewski, P.A., Rohling, E.E., Curt Stager, J., Karlén, W., Maasch, K.A., Meeker, L.D., Meyerson, E.A., Gasse, F., van Kreveld, S., Holmgren, K., Lee-Thorp, J., Rosqvist, G., Rack, F., Staubwasser, M., Schneider, R.R., Steig, E.J., 2004. Holocene Climate Variability. Quaternary Research 62, 243–255. doi:10.1016/j.yqres.2004.07.001

Moron, V., Gouirand, I., 2003. Seasonal modulation of the El Niño–Southern Oscillation relationship with sea level pressure anomalies over the North Atlantic in October–March 1873–1996. International Journal of Climatology 23, 143–155.

Moy, C.M., Seltzer, G.O., Rodbell, D.T., Anderson, D.M., 2002. Variability of El Niño/Southern Oscillation activity at millennial timescales during the Holocene epoch. Nature 420, 162–165.

Muñoz-Díaz, D., Rodrigo, F.S., 2005. Influence of the El Niño-Southern Oscillation on the probability of dry and wet seasons in Spain. Climate Research 30, 1–12.

Najac, J., Boé, J., Terray, L., 2009. A multi-model ensemble approach for assessment of climate change impact on surface winds in France. Climate Dynamics 32, 615–634. doi:10.1007/s00382-008-0440-4

Nigam, S., DeWeaver, E., 2003. Stationary waves (orographic and thermally forced).

Nuissier, O., Joly, B., Joly, A., Ducrocq, V., Arbogast, P., 2011. A statistical downscaling to identify the large-scale circulation patterns associated with heavy precipitation events over southern France. Quarterly Journal of the Royal Meteorological Society 137, 1812–1827. doi:10.1002/qj.866

Olsen, J., Anderson, N.J., Knudsen, M.F., 2012. Variability of the North Atlantic Oscillation over the past 5,200 years. Nature Geoscience 5, 808–812. doi:10.1038/ngeo1589

Orme, L.C., Reinhardt, L., Jones, R.T., Charman, D.J., Barkwith, A., Ellis, M.A., 2016. Aeolian sediment reconstructions from the Scottish Outer Hebrides: Late Holocene storminess and the role of the North Atlantic Oscillation. Quaternary Science Reviews 132, 15–25.

Ortega, P., Lehner, F., Swingedouw, D., Masson-Delmotte, V., Raible, C.C., Casado, M., Yiou, P., 2015. A model-tested North Atlantic Oscillation reconstruction for the past millennium. Nature 523, 71–74.

Peltier, W.R., Vettoretti, G., 2014. Dansgaard-Oeschger oscillations predicted in a comprehensive model of glacial climate: A "kicked" salt oscillator in the Atlantic: Dansgaard-Oeschger Oscillations. Geophysical Research Letters 41, 7306–7313. doi:10.1002/2014GL061413

Peyron, O., Magny, M., Goring, S., Joannin, S., de Beaulieu, J.-L., Brugiapaglia, E., Sadori, L., Garfi, G., Kouli, K., Ioakim, C., Combourieu-Nebout, N., 2013. Contrasting patterns of climatic changes during the Holocene across the Italian Peninsula reconstructed from pollen data. Climate of the Past 9, 1233–1252. doi:10.5194/cp-9-1233-2013

Pierre, S., Bruno, W., Francesco, F.G., Fanny, M., Jérôme, P., Anne-Lise, D., Adeline, B., Wentao, C., Cécile, P., Jean-Louis, R., Ludovic, G., Manon, B., Yves, B., Emmanuel, M., Pierre, T., Fabien, A., 2017. 6-kyr record of flood frequency and intensity in the western Mediterranean Alps – Interplay of solar and temperature forcing. Quaternary Science Reviews 170, 121–135. doi:10.1016/j.quascirev.2017.06.019

Plaut, G., Simonnet, E., 2001. Large-scale circulation classification, weather regimes, and local climate over France, the Alps and Western Europe. Climate Research 17, 303–324.

Pozo-Vázquez, D., Gámiz-Fortis, S.R., Tovar-Pescador, J., Esteban-Parra, M.J., Castro-Díez, Y., 2005. El Niño–Southern Oscillation events and associated European winter precipitation anomalies. International Journal of Climatology 25, 17–31.

Raible, C.C., Luksch, U., Fraedrich, K., 2004. Precipitation and northern hemisphere regimes. Atmospheric Science Letters 5, 43–55.

Raible, C.C., Luksch, U., Fraedrich, K., Voss, R., 2001. North Atlantic decadal regimes in a coupled GCM simulation. Climate Dynamics 18, 321–330.

Raible, C.C., Yoshimori, M., Stocker, T.F., Casty, C., 2007. Extreme midlatitude cyclones and their implications for precipitation and wind speed extremes in simulations of the Maunder Minimum versus present day conditions. Climate Dynamics 28, 409–423. doi:10.1007/s00382-006-0187-7

Raji, O., Dezileau, L., Von Grafenstein, U., Niazi, S., Snoussi, M., Martinez, P., 2015. Extreme sea events during the last millennium in the northeast of Morocco. Natural Hazards and Earth System Sciences 15, 203.

Rameau, J.-C., Mansion, D., Dumé, G., 1989. Flore forestière française: région méditerranéenne. Forêt privée française.

Randel, W.J., Wu, F., Oltmans, S.J., Rosenlof, K., Nedoluha, G.E., 2004. Interannual changes of stratospheric water vapor and correlations with tropical tropopause temperatures. Journal of the Atmospheric Sciences 61, 2133–2148.

Raynal, O., Bouchette, F., Certain, R., Séranne, M., Dezileau, L., Sabatier, P., Lofi, J., Hy, A.B.X., Briqueu, L., Pezard, P., Tessier, B., 2009. Control of alongshore-oriented sand spits on the dynamics of a wave-dominated coastal system (Holocene deposits, northern Gulf of Lions, France). Marine Geology 264, 242–257. doi:10.1016/j.margeo.2009.06.008

Reimer, P.J., Bard, E., Bayliss, A., Beck, J.W., Blackwell, P.G., Ramsey, C.B., Buck, C.E., Cheng, H., Edwards, R.L., Friedrich, M., 2013. IntCal13 and Marine13 radiocarbon age calibration curves 0–50,000 years cal BP. Radiocarbon 55, 1869–1887.

Rhein, M., 1995. Deep water formation in the western Mediterranean. Journal of Geophysical Research: Oceans 100, 6943–6959.

Rimbu, N., Lohmann, G., Felis, T., Pätzold, J., 2003. Shift in ENSO teleconnections recorded by a northern Red Sea coral. Journal of Climate 16, 1414–1422.

Roberts, N., Brayshaw, D., Kuzucuoğlu, C., Perez, R., Sadori, L., 2011. The mid-Holocene climatic transition in the Mediterranean: Causes and consequences. The Holocene 21, 3–13. doi:10.1177/0959683610388058

Roberts, N., Moreno, A., Valero-Garcés, B.L., Corella, J.P., Jones, M., Allcock, S., Woodbridge, J., Morellón, M., Luterbacher, J., Xoplaki, E., 2012. Palaeolimnological evidence for an east–west climate see-saw in the Mediterranean since AD 900. Global and Planetary Change 84, 23–34.

Rogers, J.C., 1997. North Atlantic storm track variability and its association to the North Atlantic Oscillation and climate variability of northern Europe. Journal of Climate 10, 1635–1647.

Ruiz-Barradas, A., Carton, J.A., Nigam, S., 2003. Role of the atmosphere in climate variability of the tropical Atlantic. Journal of climate 16, 2052–2065.

Sabatier, P., Bruno, W., Francesco, F.G., Fanny, M., Jérôme, P., Anne-Lise, D., Adeline, B., Wentao, C., Cécile, P., Jean-Louis, R., Ludovic, G., Manon, B., Yves, P., Emmanuel, M., Pierre, T., Fabien, A., 2017. 6-kyr record of flood frequency and intensity in the western Mediterranean Alps – Interplay of solar and temperature forcing. Quaternary Science Reviews 170, 121–135. doi:10.1016/j.quascirev.2017.06.019

Sabatier, P., Dezileau, L., 2010. Archives sédimentaires dans les lagunes du Golfe d'Aigues-Mortes. Estimation de l'aléa de tempête depuis 2000 ans. Quaternaire. Revue de l'Association française pour l'étude du Quaternaire 21, 5–11.

Sabatier, P., Dezileau, L., Briqueu, L., Colin, C., Siani, G., 2010. Clay minerals and geochemistry record from northwest Mediterranean coastal lagoon sequence: Implications for paleostorm reconstruction. Sedimentary Geology 228, 205–217. doi:10.1016/j.sedgeo.2010.04.012

Sabatier, P., Dezileau, L., Colin, C., Briqueu, L., Bouchette, F., Martinez, P., Siani, G., Raynal, O., Von Grafenstein, U., 2012. 7000 years of paleostorm activity in the NW Mediterranean Sea in response to Holocene climate events. Quaternary Research 77, 1–11. doi:10.1016/j.yqres.2011.09.002

Sabatier, P., Dezileau, L., Condomines, M., Briqueu, L., Colin, C., Bouchette, F., Le Duff, M., Blanchemanche, P., 2008. Reconstruction of paleostorm events in a coastal lagoon (Hérault, South of France). Marine Geology 251, 224–232. doi:10.1016/j.margeo.2008.03.001

Sadori, L., Giardini, M., Gliozzi, E., Mazzini, I., Sulpizio, R., van Welden, A., Zanchetta, G., 2015. Vegetation, climate and environmental history of the last 4500 years at lake Shkodra (Albania/Montenegro). The Holocene 25, 435–444.

Schroeder, K., Josey, S.A., Hermann, M., Grignon, L., Gasparini, G.P., Bryden, H.L., 2010. Abrupt warming and salting of the Western Mediterranean Deep Water after 2005: atmospheric forcings and lateral advection. Journal of Geophysical Research: Oceans 115.

Schulz, M., Stattegger, K., 1997. SPECTRUM: Spectral analysis of unevenly spaced paleoclimatic time series. Computers & Geosciences 23, 929–945.

Sgubin, G., Swingedouw, D., Drijfhout, S., Mary, Y., Bennabi, A., 2017. Abrupt cooling over the North Atlantic in modern climate models. Nature Communications 8.

Siani, G., Magny, M., Paterne, M., Debret, M., Fontugne, M., 2013. Paleohydrology reconstruction and Holocene climate variability in the South Adriatic Sea. Climate of the Past 9, 499–515. doi:10.5194/cp-9-499-2013

Sicre, M.-A., Jalali, B., Martrat, B., Schmidt, S., Bassetti, M.-A., Kallel, N., 2016. Sea surface temperature variability in the North Western Mediterranean Sea (Gulf of Lion) during the Common Era. Earth and Planetary Science Letters 456, 124–133. doi:10.1016/j.epsl.2016.09.032

Smith, A.C., Wynn, P.M., Barker, P.A., Leng, M.J., Noble, S.R., Tych, W., 2016. North Atlantic forcing of moisture delivery to Europe throughout the Holocene. Scientific Reports 6. doi:10.1038/srep24745

Solanki, S.K., Usoskin, I.G., Kromer, B., Schüssler, M., Beer, J., 2004. Unusual activity of the Sun during recent decades compared to the previous 11,000 years. Nature 431, 1084–1087.

Sorrel, P., Debret, M., Billeaud, I., Jaccard, S.L., McManus, J.F., Tessier, B., 2012. Persistent non-solar forcing of Holocene storm dynamics in coastal sedimentary archives. Nature Geoscience 5, 892–896. doi:10.1038/ngeo1619

Sorrel, P., Tessier, B., Demory, F., Delsinne, N., Mouazé, D., 2009. Evidence for millennial-scale climatic events in the sedimentary infilling of a macrotidal estuarine system, the Seine estuary (NW France). Quaternary Science Reviews 28, 499–516.

Steinhilber, F., Abreu, J.A., Beer, J., Brunner, I., Christl, M., Fischer, H., Heikkilä, U., Kubik, P.W., Mann, M., McCracken, K.G., 2012. 9,400 years of cosmic radiation and solar activity from ice cores and tree rings. Proceedings of the National Academy of Sciences 109, 5967–5971.

Stocker, T.F., Qin, D., Plattner, G.K., Tignor, M., Allen, S.K., Boschung, J., Nauels, A., Xia, Y., Bex, V., Midgley, P.M., 2013. IPCC, 2013: summary for policymakers in climate change 2013: the physical science basis, contribution of working group I to the fifth assessment report of the intergovernmental panel on climate change. Cambridge University Press, Cambridge, New York, USA.

Stuiver, M., Braziunas, T.F., 1989. Atmospheric 14C and century-scale solar oscillations. Nature 338, 405–408.

Stuiver, M., Reimer, P.J., 1993. Extended 14C data base and revised CALIB 3.0 14C age calibration program. Radiocarbon 35, 215–230.

Svendsen, L., Kvamstø, N.G., Keenlyside, N., 2014. Weakening AMOC connects Equatorial Atlantic and Pacific interannual variability. Climate dynamics 43, 2931–2941.

Torrence, C., Compo, G.P., 1998. A practical guide to wavelet analysis. Bulletin of the American Meteorological society 79, 61–78.

Trigo, I.F., Davies, T.D., Bigg, G.R., 1999. Objective climatology of cyclones in the Mediterranean region. Journal of Climate 12, 1685–1696.

Trigo, R.M., DaCamara, C., 2000. Circulation weather types and their influence on the precipitation regime in Portugal. International Journal of Climatology 20, 1559–1581.

Trouet, V., Esper, J., Graham, N.E., Baker, A., Scourse, J.D., Frank, D.C., 2009. Persistent Positive North Atlantic Oscillation Mode Dominated the Medieval Climate Anomaly. Science 324, 78–80. doi:10.1126/science.1166349

Usoskin, I.G., Gallet, Y., Lopes, F., Kovaltsov, G.A., Hulot, G., 2016. Solar activity during the Holocene: the Hallstatt cycle and its consequence for grand minima and maxima. Astronomy & Astrophysics 587, A150.

Vanniere, B., Galop, D., Rendu, C., Davasse, B., 2001. Feu et pratiques agro-pastorales dans les Pyrénées-Orientales: le cas de la montagne d'Enveitg (Cerdagne, Pyrénées-Orientales, France). Sud-Ouest Européen 11, 29–42.

Wang, C., Xie, S.-P., Carton, J.A., 2004. A global survey of ocean–atmosphere interaction and climate variability. Earth's Climate 1–19.

Winschall, A., Sodemann, H., Pfahl, S., Wernli, H., 2014. How important is intensified evaporation for Mediterranean precipitation extremes? Journal of Geophysical Research: Atmospheres 119, 5240–5256. doi:10.1002/2013JD021175

Wirth, S.B., Glur, L., Gilli, A., Anselmetti, F.S., 2013. Holocene flood frequency across the Central Alps–solar forcing and evidence for variations in North Atlantic atmospheric circulation. Quaternary Science Reviews 80, 112–128.

Woollings, T., Gregory, J.M., Pinto, J.G., Reyers, M., Brayshaw, D.J., 2012. Response of the North Atlantic storm track to climate change shaped by ocean–atmosphere coupling. Nature Geoscience 5, 313–317. doi:10.1038/ngeo1438

Xoplaki, E., 2002. Climate variability over the Mediterranean. PhD, University of Bern, Switzerland.

Zazo, C., Dabrio, C.J., Goy, J.L., Lario, J., Cabero, A., Silva, P.G., Bardají, T., Mercier, N., Borja, F., Roquero, E., 2008. The coastal archives of the last 15 ka in the Atlantic–Mediterranean Spanish linkage area: Sea level and climate changes. Quaternary International 181, 72–87.

Zielhofer, C., Fletcher, W.J., Mischke, S., De Batist, M., Campbell, J.F., Joannin, S., Tjallingii, R., El Hamouti, N., Junginger, A., Stele, A., 2017. Atlantic forcing of Western Mediterranean winter rain minima during the last 12,000 years. Quaternary Science Reviews 157, 29–51.